Journal of the Mechanical Behavior of Biomedical Materials 175 (2026) 107305

Contents lists available at ScienceDirect

Journal of the Mechanical Behavior of Biomedical Materials

journal homepage: www.elsevier.com/locate/jmbbm

Bioinspired auxetic metamaterial liners and sockets for transtibial prostheses: Energy absorption and stress redistribution

Mahdi Bodaghi [a,*,1], Saman Jolaiy [a,1], Kaveh Rahmani [a], Sheng Li [b], Fei Gao [b], Ali Zolfagharian [c]

[a] Department of Engineering, School of Science and Technology, Nottingham Trent University, Nottingham, NG11 8NS, UK
[b] Shenzhen Institute of Advanced Technology, Chinese Academy of Sciences, Shenzhen 518055, China
[c] School of Engineering, Deakin University, Geelong, VIC 3216, Australia

ARTICLE INFO

Keywords:
Prosthetics
Auxetics
Metamaterials
Liners and sockets
Finite element
3D printing

ABSTRACT

Prosthetic comfort depends on how the residual limb, liner, and socket share load. A crab-inspired auxetic metamaterial is introduced and applied to transtibial liners and sockets, with region-specific and fully auxetic variants benchmarked against conventional interfaces. Patient CT/3D scans guided anatomically targeted components. Auxetic lattices were additively manufactured in TPU (liners) and PA-12 (sockets). Cyclic compression experiments calibrated material models, and finite-element analyses quantified interface stresses and energy metrics. Across four sensitive liner regions, a four-zone auxetic TPU liner cut peak von Mises stresses by up to 60 %, and a fully auxetic liner by up to 65 %, relative to silicone/EL50 baselines. In sockets, a PA-12 design with two auxetic zones reduced peak stresses by ~40–45 % versus ABS, while a fully auxetic socket achieved ~80 % reductions with higher specific energy absorption. These findings indicate that bioinspired auxetics, integrated where anatomy needs compliance, improve pressure redistribution and mass-efficient energy management. The workflow from imaging to lattice design, printing, testing, and simulation was validated and is compatible with multi-jet fusion, enabling patient-specific prosthetic interfaces suitable for clinical translation.

1. Introduction

The rising demand for advanced lower limb prosthetics has driven innovations in socket and liner design, placing a strong emphasis on user comfort and health outcomes. Achieving effective socket design is essential for ensuring optimal pressure distribution, while liners provide crucial cushioning and stability. Nonetheless, challenges remain, including difficulties with load transfer, pressure hotspots, and maintaining thermal regulation (Wang et al., 2022; Paternò et al., 2018).

Recent studies have increasingly explored the biomechanical intricacies of the limb-socket interface. Young et al. provided a 20-year update on technologies and techniques for measuring interface mechanics, emphasizing the need for real-time pressure monitoring and customized fit solutions (Young et al., 2023). Similarly, Paternò et al. demonstrated the feasibility of embedding sensors into personalized liners, offering real-time feedback that can inform adaptive designs and improve patient outcomes (Paternò et al., 2020).

Significant progress in materials science and additive manufacturing (AM) has resulted in customized interfaces that not only improve functionality but also enhance the quality of life for amputees. Traditional prosthetic sockets have been handcrafted, relying heavily on clinician expertise and time-intensive fitting, which can lead to suboptimal outcomes due to variations in limb volume. Modern advancements such as computer-aided design (CAD), finite element analysis (FEA), and biomechanical feedback have improved socket design. The use of AM and 3D printing enables the creation of personalized solutions, while metamaterials enhance pressure redistribution and comfort. Conformal lattice metamaterials specifically reduce stress concentrations, benefiting both sockets and prosthetic liners(Wang et al., 2022; Eshraghi et al., 2013; Barreto et al., 2022; Devin et al., 2024; Brown et al., 2020; Han et al., 2025a). In low-resource settings, affordability remains a challenge; Miyata et al. evaluated sustainable, low-cost liner materials that maintain comfort and durability (Miyata et al., 2022). Adjustable sockets, reviewed by Baldock et al., offer modularity, mechanical adjustability, and smart materials to accommodate limb volume changes and enhance long-term comfort (Baldock et al., 2023). Nagarajan et al.

* Corresponding author.
E-mail address: mahdi.bodaghi@ntu.ac.uk (M. Bodaghi).
[1] Shared first authorship: Mahdi Bodaghi and Saman Jolaiy both contributed equally to this work.

https://doi.org/10.1016/j.jmbbm.2025.107305
Received 5 October 2025; Received in revised form 24 November 2025; Accepted 5 December 2025
Available online 6 December 2025

proposed single polymer composites as lightweight, robust, and AM-friendly solutions (Nagarajan et al., 2024).

Brown et al. explored limb–socket interface metamaterials for targeted pressure offloading, enabling property adjustment around bony prominences and sensitive areas (Brown et al., 2020). Broader studies emphasize the balance between performance, comfort, durability, and manufacturability in optimal designs (Price et al., 2019). Characterizations of current liners by Klute et al. revealed performance gaps that next-generation materials, such as mechanical metamaterials and thermoregulating liners, can address, particularly for active users in varying environmental conditions (Klute et al., 2010).

User needs, comfort, adjustability, cost, and aesthetics remain critical to prosthetic adoption. Emerging technologies, including AM, metamaterials, sensor integration, and predictive modeling, are advancing prosthetics toward greater performance and personalization (Manz et al., 2022; Pezzin et al., 2004; Safari et al., 2015a, 2015b; Arun et al., 2016; Basha et al., 2021; Mao et al., 2025).

Auxetic metamaterials, characterized by negative Poisson's ratios, offer tunable, lightweight, and resilient structures that improve energy absorption, anatomical conformity, and pressure distribution, enhancing overall comfort. Auxetic structures expand laterally when stretched and contract when compressed, offering advantages such as enhanced energy absorption, high shear resistance, and superior fracture toughness. First introduced by Evans in the late 1980s, though observed earlier in materials like skin and tendons, their engineered forms have advanced through improved design, modeling, and fabrication, with growing application in biomedical engineering. AM has accelerated its development, enabling novel geometries, bioinspired designs, and sustainable materials tailored for biomedical use (Ren et al., 2018; Yang et al., 2018; Kelkar et al., 2020; Meena et al., 2019; Li et al., 2019; Hasanzadeh et al., 2025; Joseph et al., 2021; Shirzad et al., 2024; Jolaiy et al., 2025; Hedayati et al., 2023; Han et al., 2022a, 2022b). Auxetic metamaterials can mimic the mechanical behavior of tissues such as skin and cartilage, improve biomechanical compatibility, and reduce stress concentrations at implant–tissue interfaces (Hasanzadeh et al., 2025; Alomarah et al., 2020a, 2020b; Quan et al., 2020). Applications include orthopedic implants, where auxetic geometries in femoral stems and spinal cages enhance micromotion distribution for osteointegration. Their conformability and cyclic load stability also suit prosthetic limb sockets, improving comfort and pressure relief (Baldock et al., 2023; Ghavidelnia et al., 2020, 2021; García-Ávila et al., 2024).

AM techniques such as fused deposition modeling (FDM), selective laser sintering (SLS), and stereolithography (SLA) enable precise fabrication of auxetic structures with controlled porosity and architecture. These methods facilitate dual-material composites, hybrid lattices, and hierarchical metamaterials with adapted properties. Innovations include fiber-reinforced auxetic honeycombs with improved strength, and 4D-printed auxetic lattices offering reversible energy absorption (Hasanzadeh et al., 2025; Joseph et al., 2021; Lvov et al., 2022; Yousefi et al., 2023; Han et al., 2025b).

Material choice is crucial for designing metamaterial structures. Thermoplastic polyurethane (TPU) offers flexibility and durability for high-strain applications, while polylactic acid (PLA) provides rigidity and biodegradability for temporary implants. Dual-material designs combining TPU and PLA improve energy absorption and fatigue performance (Ren et al., 2018; Yousefi et al., 2023; Jolaiy et al., 2024a; Namvar et al., 2022; Johnston et al., 2021; Veerabagu et al., 2022; Jiang et al., 2024).

Bioinspired strategies yield scaffolds that mimic bone and cartilage organization, promoting cell growth and vascularization. Examples such as limpet-inspired 3D/4D-printed sandwich panels demonstrate high resilience and repairability with minimal material use (Jolaiy et al., 2024b).

This study was undertaken to design and validate bioinspired auxetic interfaces for transtibial prosthetics. The goal is to reduce pressure concentrations while keeping the structures lightweight and manufacturable. A crab-inspired auxetic unit cell was integrated into four liner regions (A1-A4) and two socket regions (A5-A6). Fully auxetic liner and socket variants were also produced. A patient-specific workflow was established using CT/3D scanning with CAD to localize compliance. Cyclic compression experiments were used to calibrate TPU and PA-12 material models. Finite-element analyses showed up to ~65 % lower peak stress in liners and ~80 % in sockets, with higher specific energy absorption. These points motivate the study and frame the need for auxetic, additively manufacturable, patient-specific prosthetic interfaces.

2. Methods and materials

2.1. Sockets, linear scanning and 3D models preparation

Informed consent forms are provided to the patient before testing, and ethical approval is obtained (document number: SIAT-IRB-240315-H0713). A male patient with tibial amputation is recruited for this study. (28 years, 175 cm height, weight 70 kg, 22 years post-amputation).

We acquired image data of the patient's residual limb with a 256-row detector CT system (Revolution CT, General Electric Healthcare, USA) and used an ethylene vinyl acetate (EVA) polymer liner on the residual limb given the prevalence of soft tissue deformation when the patient underwent a CT scan in the supine position, as shown in Fig. 1a. Subsequently, we acquired CT images in DICOM format with a layer thickness of 1.25 mm and integrated the cross-sectional images using MIMICS software to create a comprehensive 3D model. We categorized skin, fat, and muscle as soft tissue and omitted nonessential components such as meniscus, cartilage, and ligaments from the analysis. The bone and limb models are segmented according to different grayscale values (bone: 90–1703; limb tissue: 150-1703), as shown in Fig. 1(b and c). Additionally, the original 3D model of the patient's prosthetic socket is obtained using 3D scanning (Markscan Lite, HEXAGON), as shown in Fig. 1d. Furthermore, the above model exhibits defects such as tiny holes and protrusions. Therefore, subsequent shape processing is performed on the models above. Initially, the bone models are separated into femur, patella, tibia, and fibula components. Subsequently, protrusions are eliminated through removing spikes operations on the respective models, and the surfaces are smoothed and repaired utilizing noise reduction, relaxation, and sanding. This step is crucial for meshing the models in subsequent FEA. Among them, over the tibial crest (A1), the distal tibial end (A2), the fibula ends (A3), and the patellar bone (A4) are the pressure-sensitive regions in the residual limb. Then, use Boolean operations to remove the skeleton from the residual limb to obtain the residual tissue, and thicken the soft tissue model by 5 mm to obtain the liner model. Additionally, the 3D scanning prosthetic socket model is also optimized. In particular, the force-sensitive areas such as the tibia and the residual limb bottom (A5-A6) require greater attention to enhance comfort. Finally, the processed bone and limb models are surface-fitted to acquire solid models in STP format.

A limitation of the current study is its reliance on a single patient, which constrains the generalizability of the findings. Future research should encompass a larger and more diverse cohort to validate the proposed auxetic liner and socket designs across different anatomies, amputation levels, and post-amputation histories. This approach would enhance the applicability and robustness of the results.

2.2. Conceptual design & auxetic unit cell design

As illustrated in Fig. 2, the proposed novel auxetic structure introduced in this study is inspired by the morphological characteristics of a crab. The configuration features a centrally located crab body core from which four symmetric branches extend outward. This bio-inspired design aims to achieve a tunable mechanical response by leveraging geometrical re-entrant features, which are known to induce auxetic

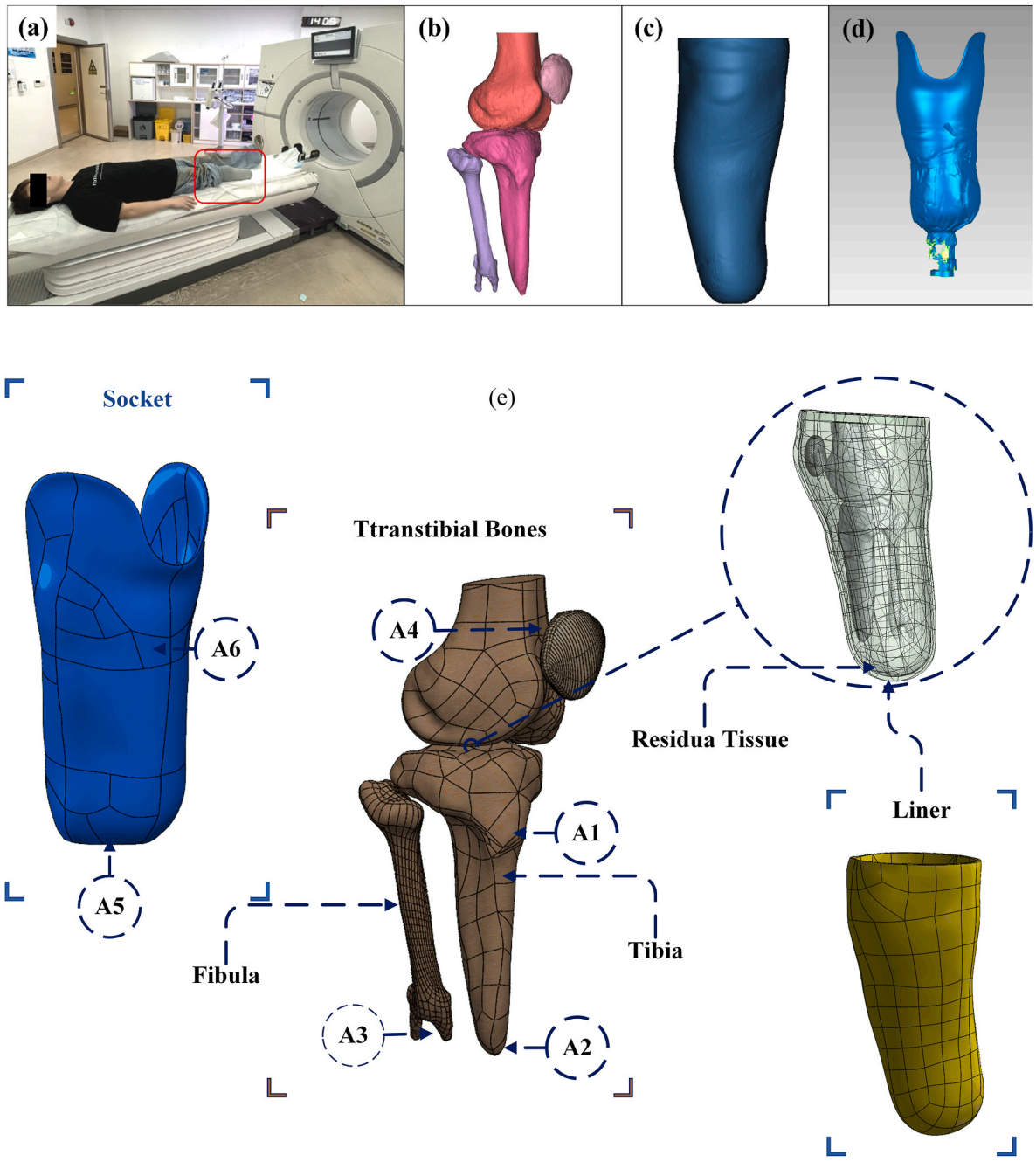

Fig. 1. Construction of the residual limb model. (a) CT pictures, (b) bone model, (c) limb model, (d) socket model, (e) Smoothed residual tissue, transtibial bone, liner, and socket, with the important area A1-A6.

effects. Further details of the geometric dimensions and configuration are provided in Fig. 2. It is observed that upon application of a uniaxial displacement in the vertical direction, the structure exhibits a lateral contraction along the horizontal axis. This transverse compression under longitudinal tension indicates a negative Poisson's ratio, confirming the auxetic nature of the proposed architecture. Such behavior is particularly advantageous in applications requiring conformal fitting, energy absorption, or tunable stiffness, making this design highly relevant for integration in biomechanical systems such as sockets and liners.

A set of geometrical parameters defines the morphology of a crab leg: "L_1" to "L_4", "θ_1" and "θ_2", and "t". The parameter "t" denotes the overall thickness of the structure. Parameters "L_1" and "L_2" represent the main lengths of the unit cell, "L_3" is the length of the inner star shape, while "L_4" refers to the length of the arms extending from the central structure. The unit cell is designed to be fully symmetrical to ensure uniform mechanical behavior during compression.

Given the inherently small scale of typical prosthetic liners and sockets, direct physical evaluation of the proposed auxetic architecture at its intended anatomical dimensions would have posed significant challenges in terms of fabrication, instrumentation, and mechanical testing. To address these constraints and facilitate experiential validation of the auxetic response, the structure is geometrically scaled to macroscopic dimensions suitable for laboratory prototyping. Specifically, the values used in this design to create the 3D model for 3D printing are $L_1 = 26$ mm, $L_2 = 20$ mm, $L_3 = 9.75$ mm, $L_4 = 5$ mm, $\theta_1 = 45^\circ$, $\theta_2 = 34^\circ$, and $t = 1$ mm. Accordingly, a rectangular-cube-shaped model with overall dimensions of $62 \times 62 \times 50$ mm^3 is developed as a physically realizable test specimen.

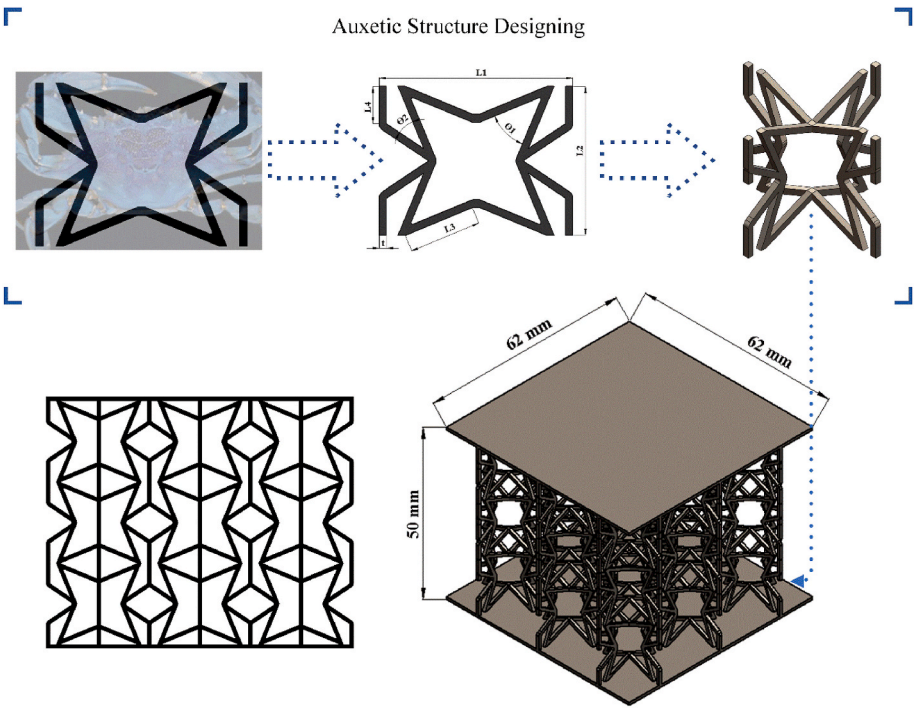

Fig. 2. The designed unit cell mimicking the shape of a crab, the final auxetic structure is designed by using this unit cell with their dimensions.

As illustrated in Fig. 2, the enlarged auxetic construct has been modeled in SolidWorks utilizing a pattern tool. Initially, two novel mutually compatible two-dimensional unit cells inspired by the articulated configuration of a crab are integrated perpendicularly to form a 3D unit cell. This 3D unit cell serves as the fundamental building block for the final lattice structure. Next, we replicate the 3D unit cell along the X, Y, and Z axes using pattern-generation tools in SolidWorks to create the complete lattice volume. We apply three repetitions in each spatial direction, resulting in a total of 27 distinct three-dimensional unit cells in the final structure. Since each 3D unit cell includes two underlying 2D unit cells, the entire lattice consists of 27 three-dimensional units, equating to 54 two-dimensional sub-units.

The design process focuses on enhancing manufacturability through additive methods, ensuring that the final geometry is free from overhangs that would require support. It incorporates continuous, interlocking re-entrant shapes that align with auxetic kinematics. The final model is designed for compatibility with standard FDM 3D printers, making it ideal for rapid prototyping and subsequent mechanical testing under controlled loading conditions.

2.3. Materials

This study presents the development of advanced three-dimensional bio-mimetic auxetic lattices design for prosthetic socket-liner systems, wherein soft thermoplastic elastomers are employed for the liner layer and rigid polymeric materials for the socket framework.

For the rigid components of the prosthetic socket and the hybrid auxetic lattice supports, PA12 is chosen for its capacity to endure significant loads while maintaining both dimensional stability and rigidity, as well as its ability to effectively dissipate impact energy. In contrast, TPU is selected for the prosthetic liners due to its hyperelastic characteristics and excellent energy dissipation, which provide efficient damping and rapid recovery during repeated loading cycles. These material selections ensure a harmonious balance between structural integrity, manufacturability, and biomechanical performance within the proposed auxetic prosthetic system.

Both material types are fabricated via Multi Jet Fusion (MJF) AM, enabling the precise realization of intricate geometries and designed mechanical gradients.

Comprehensive mechanical evaluations, including monotonic and cyclic loading-unloading protocols, demonstrate that TPU-based structures are capable of sustaining substantial elastic deformation while exhibiting excellent shape-memory behavior. In contrast, PA 12 revealed a characteristic elastoplastic deformation with measurable residual strains, alongside pronounced energy absorption capacity under repetitive loading.

Confirming the reliability of the obtained mechanical data, the stress-strain profiles for both PA 12 and TPU are depicted in Fig. 3a and b, respectively. The mechanical characteristics of PA 12 are investigated through quasi-static uniaxial tensile testing to better understand its structural behavior under load. As illustrated in Fig. 3a, PA 12 exhibits an initially linear elastic response up to a stress threshold of approximately 30 MPa. This linear area corresponds to the reversible elastic deformation range, within which the material promptly returns to its original shape upon unloading. The stress-strain trajectory confirms that PA 12 can endure appreciable loads before undergoing structural failure, making it well-suited for applications where dimensional stability, rigidity, and impact energy dissipation are crucial, such as rigid prosthetic socket frameworks or structural lattice supports in hybrid auxetic systems. As shown in Fig. 3b, TPU exhibits a distinctly nonlinear and hyperelastic response under uniaxial tension. The initial loading trajectory (Path A) progresses up to the peak strain point, followed by an unloading path (Path B) that deviates below the original curve, thus forming a clear hysteresis loop (Cycle 1). This divergence between loading and unloading curves within the first cycle reflects a stress softening phenomenon, whereby the unloading stress at a given strain is lower than the corresponding loading stress, indicative of internal energy dissipation mechanisms inherent to soft elastomeric materials.

Moreover, TPU displays remarkable elasticity, enduring substantial strains while fully recovering to its original shape without exhibiting any measurable residual deformation. The second loading–unloading sequence further elucidates the mechanical response: reloading up traces a new intermediate path (Path C), positioned between the initial loading and unloading curves, while the subsequent unloading (Path D)

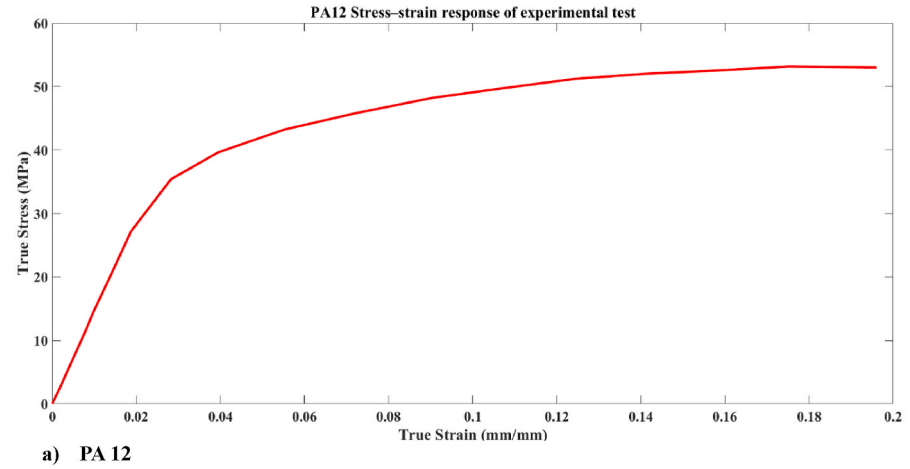

Fig. 3. The result of the mechanical behavior of PA12 and TPU in the experimental test.

retraces the original Path B. This progressive shift in mechanical behavior, marked by reduced stiffness and persistent hysteresis, is a hallmark of the Mullins effect, commonly observed in filled or cross-linked elastomers subjected to repeated deformation cycles. The Mullins effect describes the phenomenon of stress softening observed in rubber-like and hyperelastic materials, such as TPU, when subjected to repeated loading and unloading cycles. During the initial loading cycle, the material displays its highest stiffness. However, in subsequent cycles, it exhibits lower stress levels at the same strain, meaning it becomes softer once it has been stretched. Notably, the unloading path in each cycle tends to follow the same curve as in previous cycles, which is a key characteristic of the Mullins effect.

These findings highlight the hyperelastic nature of TPU and its pronounced energy dissipation capabilities, making it a suitable candidate for prosthetic liner applications where damping and recovery are critical.

2.4. 3D printing process

Specimens were printed using an HP Multi Jet Fusion (MJF) 5200 3D printer with HP 3D TPU powder. The process utilized a blend of 80 % recycled and 20 % virgin powder, alongside the recommended balance printing and normal cooling settings. After printing, the components were left to cool in the build chamber overnight. Subsequent to removal, bead blasting was performed to eliminate any residual powder from the specimen surfaces.

2.5. Experimental tests

In this study, auxetic structures, as shown in Fig. 4a, were fabricated using HP MJF 3D printing and tested under compression. Mechanical performance was evaluated under cyclic loading–unloading at a constant crosshead speed of 10 mm min^{-1}. Compression tests were performed on a Shimadzu AG-X Plus universal testing machine. It test was conducted at 23 °C and 50 % relative humidity (standard laboratory conditions).

3. Simulation validation

In order to support the experimental findings, a comprehensive computational model has been developed within the ABAQUS environment. This study validates the simulation through experimental testing of the cubic auxetic structure. Future research will focus on conducting mechanical tests of the prosthetic interfaces under simulated gait conditions, thereby complementing the finite element simulations. These experiments are anticipated to provide deeper insights into the mechanical performance, comfort, and durability of the proposed auxetic liner and socket designs in practical usage scenarios.

3.1. Materials

The hyperelastic behavior of TPU and the elastoplastic response of PA 12 are modeled using appropriate material constitutive models, incorporating the Mullins effect formulation to simulate large-strain behaviors of TPU accurately.

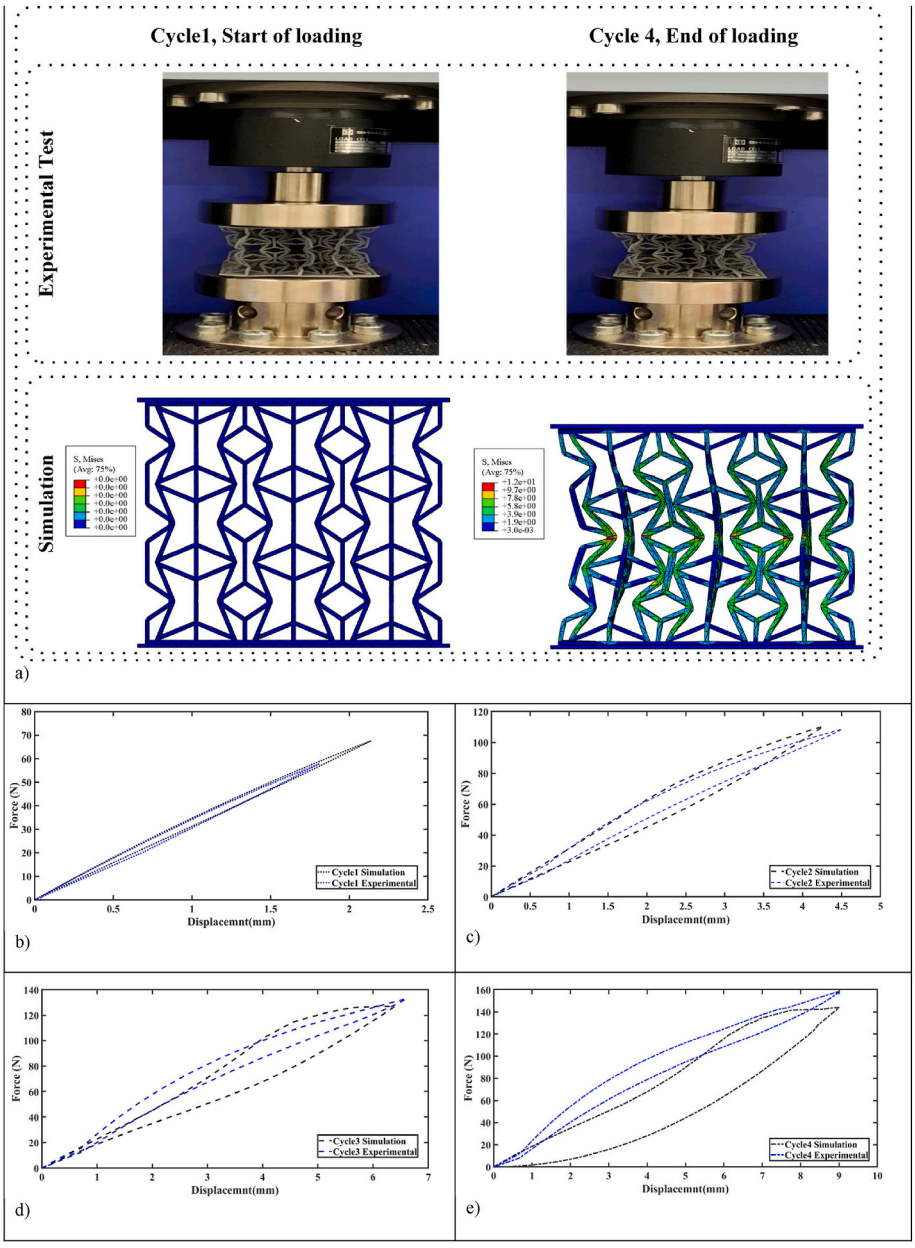

Fig. 4. The simulation validation process: a) Experimental compression test and simulation compression tests, b-e) Displacement-Force for both experimental test and simulation in 4 cycles for the final auxetic structure.

To accurately characterize the material responses, the experimental stress–strain data for both TPU and PA 12 are directly imported into ABAQUS using the Calibration utility, which automatically fits the appropriate material model and generates the corresponding material property definitions.

For PA 12, an elastic–plastic material model is applied to capture the observed yield behavior and strain hardening seen during uniaxial testing. In contrast, the hyperelastic nature of TPU, along with its stress-softening under cyclic loads, necessitates a more advanced approach. The Mooney–Rivlin hyperelastic model is adopted to represent TPU's nonlinear response, with material parameters calibrated from experimental data using the Evaluate Materials module. To simulate the cyclic stress-softening phenomenon, commonly referred to as the Mullins effect, ABAQUS's inbuilt Mullins damage feature is activated. This feature enables the model to replicate the progressive reduction in stress upon reloading, where the material follows the unloading path of the previous cycle, a behavior observed in elastomeric materials subjected to repeated deformation.

This study also includes conventional materials, Silicone and EL50 for the liner, and ABS for the socket, to establish a comparative benchmark against the newly proposed structures. These materials have been extensively utilized in prior research involving non-auxetic liner and socket systems. By incorporating them into the current simulations, we can critically assess the mechanical performance of the innovative auxetic designs in relation to established standards. A summary of the mechanical properties of all materials used in this investigation can be found in Table 1.

In this study, a comprehensive finite element analysis is conducted to investigate the cyclic mechanical behavior of novel auxetic structures fabricated from thermoplastic materials. The 3D final auxetic structure, with dimensions of $62 \times 62 \times 50$ mm^3, is initially designed using SOLIDWORKS CAD software and subsequently imported into the ABAQUS simulation environment for mechanical analysis under compressive cyclic loading conditions, replicating the experimental protocols.

Table 1
Material properties used in FEA(Barreto et al., 2022; Devin et al., 2024; Bates et al., 2019).

Component	E (MPa)	η	ρ(g/cm^3)	application
Silicone	0.28	0.49	1.05	liner
ABS	1290	0.3	1.15	Socket
EL50	2.63	0.49	1.15	Liner
PA12	Fig. 3a	0.35	0.92	Socket
TPU	Fig. 3b	0.48	1.2	Liner

3.2. Simulation method

The investigation of auxetic structures necessitated the use of the Dynamic Implicit solver due to the substantial deformations, nonlinear material behavior, and intricate contact interactions inherent in these materials. This solver is characterized by its numerical robustness, making it ideally suited for simulations that involve significant geometric nonlinearity and complex contact scenarios. To maintain a quasi-static analysis and to prevent the influence of dynamic effects, the loading rate was deliberately set to a low value, which reduced inertial contributions. Additionally, the quasi-static option was explicitly selected within the Application settings of the Dynamic Implicit step in ABAQUS. The Dynamic Implicit procedure is activated via the step module, enabling geometric nonlinearity (NLGEOM), with the increment control set to Fixed and Global. The simulated model includes three main components: a rigid upper loading plate (movable jaw), the auxetic structure, and a rigid lower fixed plate (fixed jaw). The upper and lower jaws are defined as rigid bodies through reference points using the Interaction Module, allowing the extraction of reaction forces and displacement data with high reliability. General contact interactions are implemented across all interfaces, accommodating both normal and tangential frictional behavior during loading and unloading cycles.

3.3. Meshing

A mesh convergence analysis is conducted to determine the optimal element density for achieving reliable simulation outcomes across all simulations. Given the intricate geometry of the final auxetic design, the Free Tetrahedral element configuration is selected within the Mesh Control section, applying an Element Growth Rate of 1.05. To accurately represent the hyperelastic behavior of thermoplastic polyurethane (TPU), a 4-node linear tetrahedral element with hybrid pressure formulation (C3D4H) is utilized. The hybrid pressure formulation is essential for accurately modeling nearly incompressible materials such as TPU. Standard displacement-based finite elements often encounter issues of volumetric locking when addressing incompressible or hyperelastic behaviors. By incorporating an additional pressure degree of freedom, hybrid elements enable a more precise representation of both the volumetric and deviatoric responses of the material. The average mesh size is established at 1 mm, with a maximum curvature deviation of 0.05, enhancing mesh fidelity in geometrically complex regions. Approximately 134,000 elements are generated throughout the auxetic structure, which is deemed the minimum mesh density necessary to yield a stable and reliable force–displacement response. This methodology is consistently applied across all simulated components in this study to ensure that the results are independent of the mesh used.

The upper and lower jaws of the testing assembly are discretized using reduced-integration linear hexahedral elements (C3D8R), ensuring adequate rigidity for simulating quasi-rigid boundaries. The final meshed configuration and the outcomes of the mesh sensitivity study are presented in Fig. 4a and b, respectively. These confirm the precision and efficiency of the meshing strategy, reinforcing the credibility of the simulation model in replicating the cyclic mechanical behavior of auxetic metamaterials under compressive loading.

3.4. Validation

Fig. 4 presents a thorough comparison of the experimental results and finite element simulations concerning the auxetic specimen subjected to compressive cyclic loading. As illustrated in Fig. 4a, the deformation states of the sample are depicted at the commencement of the first cycle and after the fourth cycle, just before unloading. The left image represents the undeformed configuration before loading, while the right image showcases the specimen at its maximum deformation at the end of the fourth loading cycle. These experimental images are compared with the stress-distribution results derived from finite element analysis in ABAQUS, demonstrating a strong visual correspondence between the physical and simulated deformations.

In Fig. 4a, the von Mises stress distribution obtained from finite element analysis (FEA) is displayed at two pivotal stages of the cyclic compression process: the initial undeformed state before the first loading cycle (left) and the fully deformed state after the fourth loading cycle (right). It is evident from the figure that the structure experiences considerable vertical compression, accompanied by lateral contraction in the transverse direction. This lateral shrinkage under axial compression distinctly indicates the auxetic nature of the designed metamaterial, characterized by a negative Poisson's ratio.

Fig. 4b–e depicts the force–displacement curves for all four loading cycles, comparing the numerical predictions from the ABAQUS simulations with the corresponding experimental results. In the first cycle, the simulation forecasts a peak compressive force of approximately 70 N at a displacement of 2 mm, while the experimental counterpart records roughly 60 N. During the second cycle, the simulation indicates a force just above 100 N at 4 mm displacement, aligning closely with the experimental data, which is also approximately 100 N. In the third cycle, the simulation curve reaches slightly below 120 N at 6.5 mm, whereas the experimental test yields a marginally higher value of just above 120 N. Finally, in the fourth cycle, the experimental test reveals a maximum compressive force of approximately 160 N at a 9 mm displacement, with the simulation yielding a corresponding force of about 140 N.

In summary, the simulated force–displacement response exhibits a strong correlation with experimental observations, both in magnitude and trend, thereby validating the fidelity of the finite element model employed in this study. These findings confirm that the numerical approach implemented in ABAQUS serves as a reliable tool for predicting the mechanical behavior of auxetic metamaterials under cyclic compressive loading.

4. Auxetic structure design for liner and socket

4.1. Selecting sensitive anatomical areas in the liner and socket

Following the validation of the simulation results through comparison with experimental data, the design process proceeded with the anatomical customization of the auxetic structures. This stage is informed by the biomechanical characteristics and geometric contours of a transtibial amputated limb to achieve improved load distribution and pressure relief in the prosthetic interface.

Based on insights from the previous studies(Barreto et al., 2022; Devin et al., 2024; Brown et al., 2020; Plesec et al., 2023; Fardan et al., 2023). Anatomically driven partition of the residual limb is performed to optimize the spatial deployment of auxetic structures in the liner and socket. This study highlights that custom-designed metamaterial liners significantly improve pressure distribution compared to homogeneous liners by locally designing mechanical responses in anatomically distinct areas. To maximize anatomical conformity and biomechanical performance, six distinct anatomical areas (A1–A6) are designated for embedding auxetic mechanical metamaterials in the transtibial prosthetic system. Four areas (A1–A4) are allocated to the prosthetic liner, while two areas (A5–A6) are embedded in the socket. Notably, area A6 in the socket corresponds anatomically to area A1 in the liner, both

addressing the tibial crest area.

Area A1 lies directly over the tibial crest, a superficial bony prominence with minimal soft tissue coverage. It is highly susceptible to discomfort and skin breakdown under axial loading. An auxetic layer with high lateral expandability is embedded to reduce localized pressure concentrations and improve comfort. Area A2 is located just above the distal tibial end, where the bone's sharp termination often generates high pressure during stance and push-off. Auxetic patterns in this Area increase compressibility and distribute forces more evenly over the stump. Area A3 overlays the lateral side of the residual limb where the fibula ends. It is a common location for socket-induced irritation due to lateral movements and minimal cushioning. An auxetic unit cell structure is introduced to provide shock absorption and lateral compliance. Area A4 corresponds to the patellar bone, which is prominent and sensitive to pressure and motion, particularly during knee flexion. The designed auxetic layer enhances local adaptability and minimizes restriction in the knee's range of motion. Area A5 in the socket is located beneath the anterior-distal tibia and lateral fibular areas (A2 and A3); this area corresponds to the posterior curvature of the residual limb near the gastrocnemius insertion. Soft tissues here deform considerably during walking. An auxetic Area with low stiffness and high resilience is used to accommodate volumetric changes and maintain comfortable pressure distribution. Area A6 directly faces and mirrors A1 in the liner. It overlays the tibial crest and is often subjected to compressive forces in rigid socket designs. An embedded auxetic core within the socket's anterior wall is used to reduce the stress concentration and enhance energy return during gait.

As illustrated in Fig. 5, six distinct auxetic components are designed and assigned to specific anatomical areas of the liner and socket. Among these, components A1 to A4 correspond to the prosthetic liner and are designed with unique dimensions and shapes according to their anatomical locations. In contrast, components A5 and A6 are embedded within the socket structure. The anatomical partition is based on prior studies identifying high-stress areas during gait cycles, such as the anterior crest of the tibia and the distal ends of the tibia and fibula.

All A1-A4 and A6 components are designed using rotationally patterned auxetic unit cells. To achieve this, a single unit cell geometry is revolved around a central axis using the "Revolve" feature in SolidWorks, creating a cylindrical auxetic part. The radial dimensions and angular sweep of each revolved cell are adjusted according to the anatomical coverage required in each area. For the vertical construction of each component, the revolved unit cell is vertically patterned to match the desired height of the anatomical area within the liner or socket.

This modular approach enabled precise geometric control and tuning of auxetic behavior for each part, allowing differential compliance and stress distribution at the interface between the residual limb and the prosthetic socket. The structural parameters of the revolved auxetic components are specifically optimized, as shown in Table 2, for the local biomechanical requirements of each area, ensuring enhanced comfort, fit, and mechanical performance under cyclic loading.

As shown in Fig. 5, component A5 of the socket is uniquely designed to embed a rectangular auxetic block within a hemispherical outer shell. This design serves a dual biomechanical purpose. On one hand, it directly supports the distal ends of the tibia and fibula, corresponding to anatomical areas A2 and A3, ensuring that these sensitive bony prominences are cushioned during load transfer. On the other hand, the hemispherical geometry facilitates seamless attachment to the prosthetic shank, which in turn connects the socket to the foot and transmits forces to the ground.

The rectangular auxetic core within the hemispherical casing is specifically engineered to enhance energy absorption in this high-stress

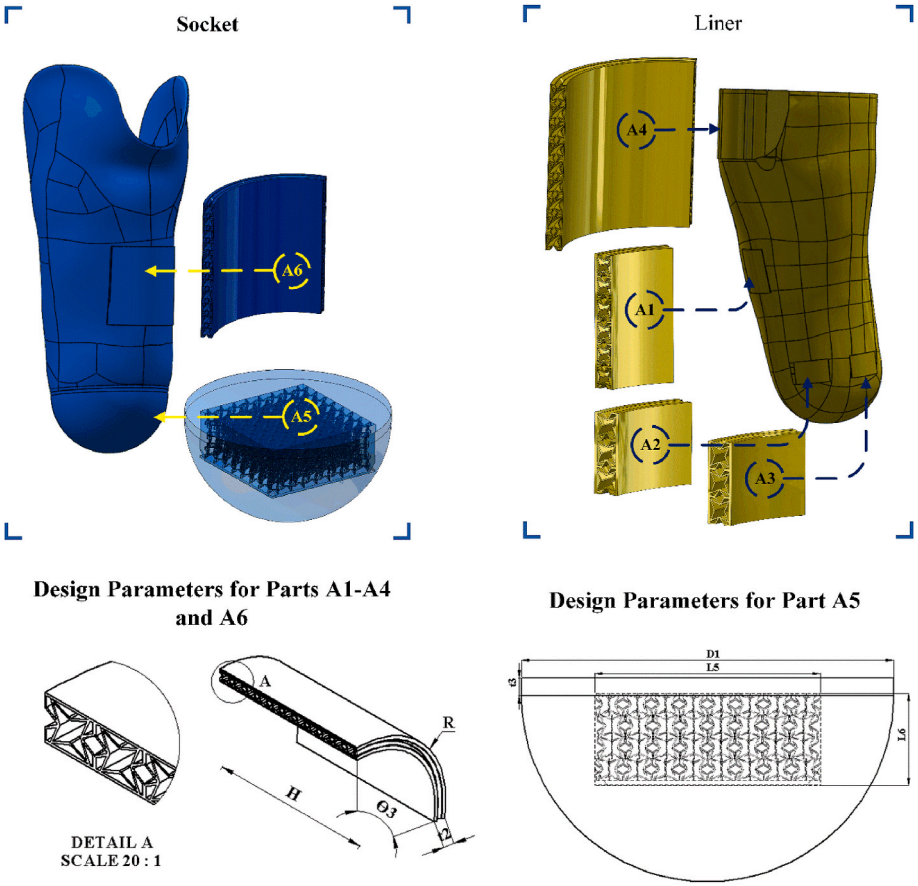

Fig. 5. The shape, location, and design parameters of all parts A1-A6 in the liner and socket.

Table 2
The dimensions of the designed parts A1-A4 and A6, with the dimensions of their unit cell.

Part Name	Part Design				Unit Cell Design					
	R(mm)	H(mm)	Θ_3(deg)	t_2(mm)	L_2(mm)	L_3(mm)	L_4(mm)	Θ_1(deg)	Θ_2(deg)	t(mm)
A1	32	32	38	5	4	1.95	1	45°	34°	0.5
A2	45	16	30	5	4	1.95	1	45°	34°	0.5
A3	45	16	30	5	4	1.95	1	45°	34°	0.5
A4	35	50	95	5	4	1.95	1	45°	34°	0.5
A5					8	3.9	2	45°	34°	1
A6	37	58	100	5	4	1.95	1	45°	34°	0.5

area. By utilizing an auxetic configuration, the structure can deform in a controlled manner under compression, thereby reducing peak stresses transmitted to the residual limb at the distal tibia and fibula. This geometry not only optimizes load distribution but also enhances the comfort and safety of the user during locomotion.

For the cylindrically shaped elements (A1 to A4 and A6), four principal parameters are employed: the outer radius (R), which dictates the radial span and determines conformity to the limb's cross-sectional profile; the angular sweep (θ) of the revolved unit cell, which defines the circumferential extent of each pattern; the wall thickness (t_2), which influences the local stiffness and energy absorption characteristics; and the vertical height (H), adjusted individually for each component to match the corresponding part of the residual limb. These parameters allowed for precise modulation of the auxetic response across varying anatomical locations.

In contrast, the geometry of component A5, located at the distal base of the socket, is defined using a distinct set of parameters due to its hybrid structure, consisting of a rectangular auxetic block embedded within a hemispherical shell. The diameter of the hemisphere ($D_1 = 85$ mm) sets the curvature for distal conformity, while the internal block is described by its length (L_5), width ($W_5 = L_5 = 70$ mm), and height ($H_6 = 20$ mm), which are tuned to cover the contact areas beneath the tibial and fibular ends. An additional cylindrical extension is incorporated above the hemisphere with a thickness ($t_3 = 4$ mm), not for mechanical performance, but to ensure smooth interfacing with the ends of area A2 and A3. Collectively, these parameters enabled the development of highly specialized components capable of achieving localized stress relief, anatomical adaptation, and mechanical reliability in both static and dynamic prosthetic loading conditions.

In addition to the modular components A1 through A6, each specifically designed to anatomically significant areas of the transtibial residual limb, this study introduces a novel auxetic socket concept, designed entirely using a newly developed unit cell inspired by the skeletal morphology of a crab shape. As illustrated in Fig. 6, the socket is composed of a fully revolved auxetic architecture, where the unit cells are rotationally patterned to form a continuous, conformal, and mechanically responsive structure. The dimensions of the unit cell are the same as are used for parts A1-A4 and A6. Unlike conventional designs, the diameter of this socket varies along its vertical axis, precisely reflecting the complex anatomical taper of the residual limb, which is first encased by the liner and subsequently by the socket. The dimensions of the full auxetic-designed socket are shown in Fig. 7. The thickness of the socket is 5 mm. For the full auxetic liner, the same dimensions are used by subtracting the thickness of the socket. This spatially adaptive and structurally auxetic configuration enables not only enhanced mechanical integration with the limb but also the potential for improved energy dissipation, pressure distribution, and long-term user comfort.

5. Results and discussion

This study investigates the influence of auxetic metamaterial

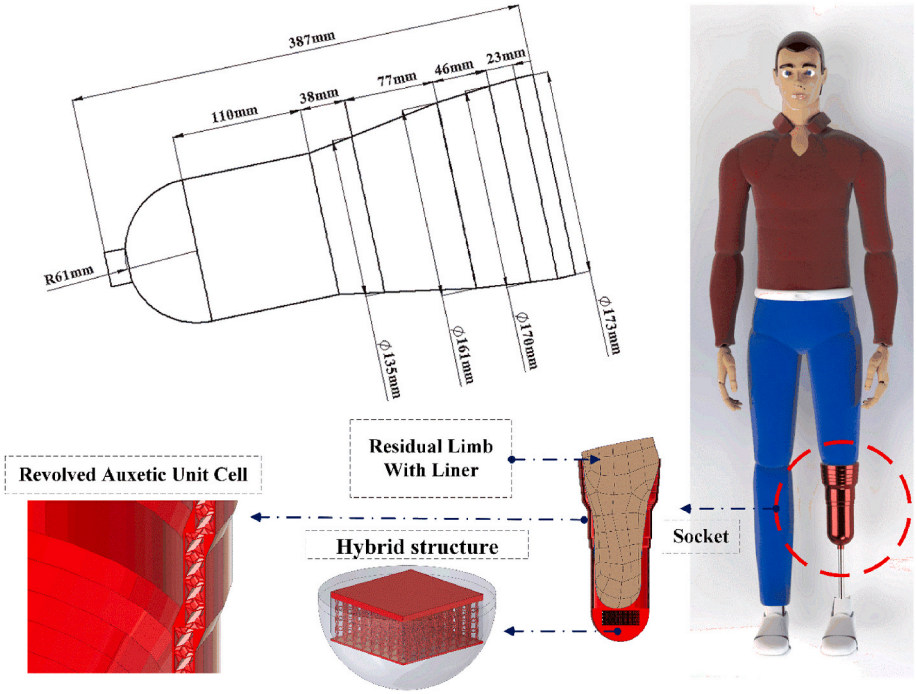

Fig. 6. The shape and dimensions of the full auxetic-designed socket.

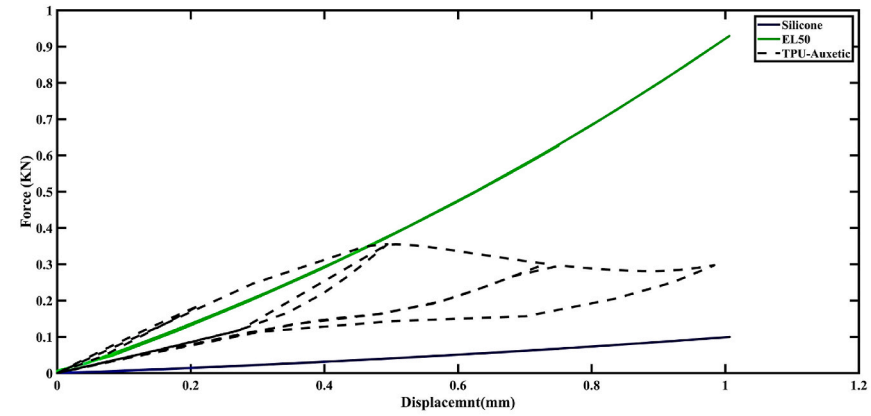

a)

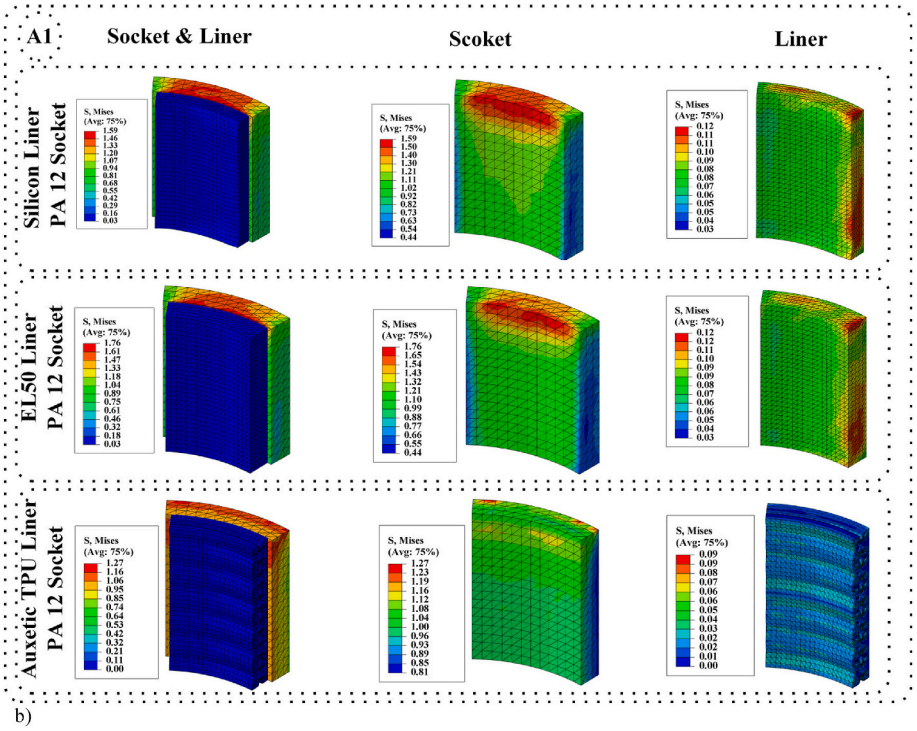

b)

Fig. 7. Simulation results for Part A1, a) Force-Displacement under 20 % strain, b) Von Mises stress distribution for the sample liner with Silicone and material, and EL50 auxetic liner with TPU material and socket with PA12 material.

structures on stress distribution within prosthetic liners and sockets. To thoroughly assess the performance and contribution of each component, all six designed parts (A1 through A6) are included in the simulation, as well as the full auxetic socket and full auxetic liner.

The geometric models of the customized components are initially designed using SolidWorks and subsequently imported into the ABAQUS simulation environment as individual parts. Once imported, appropriate mechanical properties are assigned to each part based on previously calibrated material data. Specifically, for the liner, three different material types are examined: silicone, Elastic 50A (EL50) (an elastomeric polyolefin commonly used in prosthetic applications), and TPU. The auxetic-enhanced liner parts (A1 to A4) are exclusively modeled using TPU, a material known for its recoverable large deformation behavior and high energy dissipation capability. For the socket, two types of materials are considered: PA12 for the auxetic structure and ABS for the conventional socket. (Paternò et al., 2018).

To comprehensively evaluate the efficacy of the auxetic design, stress distribution results from the TPU-based auxetic liners are compared against conventional non-auxetic liners made of EL50 and silicone, as commonly reported in previous studies (Devin et al., 2024). This comparative analysis provided quantitative insight into how auxetic topology, in conjunction with advanced material selection, improves load distribution and reduces stress concentration in critical anatomical Areas.

To evaluate the performance of the proposed auxetic structure simulated with TPU, a comparative analysis is conducted against conventional liners made of Silicone and EL50. Two sets of comparative assessments are performed. The first focused on quantifying the energy absorption and dissipation capacities of the liners under repeated cyclic loading.

The energy dissipation (ED) and energy absorption (EA) values are extracted from the area under the loading and unloading curves for each cycle. The comparative results obtained from the simulation are summarized in Table 3.

For all analyzed structures, tetrahedral meshing is implemented within the ABAQUS finite element environment to accommodate the

Table 3
Dissipated energy, absorbed energy, and SEA for parts A1-A6 with different materials.

Sample Number	m(g)	Absorbed Energy (J)	SEA (J/g)	m(g)	Absorbed Energy (J)	SEA (J/g)	m (g)	Dissipated energy (J)	Absorbed Energy (J)	SDE(J/g)	SEA (J/g)
LINER	Silicone			EL50			Designed Auxetic Structure				
PART A1	4.96	0.044	0.009	4.96	0.74	0.15	1.75	0.11	0.43	0.07	0.24
PART A2	1.7	0.039	0.023	1.7	0.29	0.17	0.60	0.12	0.41	0.20	0.69
PART A3	1.7	0.039	0.023	1.7	0.29	0.17	0.60	0.12	0.41	0.20	0.69
PART A4	15.000	0.326	0.022	15	3.13	0.21	5.29	0.24	0.75	0.04	0.14
Socket	ABS			Designed Auxetic Structure							
PART A5	94.000	9.469	0.101	53.000	7.22	0.14					
PART A6	18.000	29.103	1.617	1.850	13.23	7.15					

complex geometries of the models. A maximum global element size of 1 mm is consistently applied across all parts to ensure sufficient resolution for capturing local stress distributions without excessive computational time.

Specifically, for components simulated with TPU, the hybrid linear tetrahedral element type C3D4H is selected. This choice is based on the hyperelastic behavior of TPU, for which hybrid elements offer improved numerical stability and accuracy in simulating nearly incompressible materials under large deformations. For components composed of other materials, such as EL50, silicone, PA12, and ABS, standard C3D4 elements, four-node linear tetrahedra, are employed, as these materials exhibit different mechanical responses that do not necessitate a hybrid formulation.

The adoption of these meshing strategies ensures reliable force–displacement predictions under nonlinear loading conditions and supports convergence in simulations involving both elastoplastic and hyperelastic materials.

Force–displacement curves are obtained for all designed linear structures under compressive strain levels reaching up to 20 %, which corresponds to typical deformations encountered during gait cycles. Considering the cyclic nature of human locomotion, loading is applied across four consecutive cycles to mimic realistic conditions.

Due to the hyperelastic nature of TPU and the incorporation of the Mullins effect into the numerical model using the Mooney–Rivlin formulation, the TPU-based auxetic liners can exhibit both energy absorption and hysteresis responses characteristic of soft rubber-like materials. Equivalent loading protocols are implemented for the EL50 and silicone liners to ensure consistency across the simulation.

To assess and compare the stress distribution within the engineered structures, an equivalent total force of 850 N is applied to each model in the pressure-loading section within ABAQUS. Although this applied force significantly exceeds the surface pressure of 220 kPa, commonly cited in previous studies (Barreto et al., 2022; Devin et al., 2024), it is intentionally chosen to represent a worst-case loading condition. This load approximates the full body weight acting directly on each anatomical part (A1–A6), assuming complete weight-bearing through the prosthetic interface. Such an approach enables robust structural assessment under maximum mechanical demand.

For all parts A1 through A4, where both liner and socket are modeled simultaneously, with PA-12 material for the sockets. Notably, part A4 is analyzed solely in the context of the liner due to its anatomical location. Parts A5 and A6, which are a section of the socket, are modeled with a TPU-based liner and a PA-12 socket in the auxetic configuration. This consistent material pairing across configurations enables a direct and comprehensive assessment of the structural and biomechanical advantages offered by auxetic metamaterial integration in prosthetic design.

For components A1, A2, A3, and A6, identical boundary conditions are established utilizing a cylindrical coordinate system. The left and right lateral faces of these components are constrained by fixing the displacement in the circumferential (θ) direction, thereby preventing any rotational or tangential movement. Furthermore, the top and bottom surfaces of each component experienced restrictions through the imposition of zero radial and axial (z-axis) displacements. In a manner consistent with these components, the boundary constraints for A4 are also defined within a cylindrical coordinate framework. However, distinct from the preceding components, the upper surface of A4 is left unrestrained, allowing it to remain entirely free during the simulation. This design choice was made to better represent its physiological interaction with the surrounding soft tissues. The lower surface of A5, which denotes the connection to the socket structure, was assigned an ENCASTRE (fully fixed) boundary condition in ABAQUS, thereby constraining all translational degrees of freedom.

5.1. Liner Area A1

As illustrated in Fig. 7a, force–displacement curves for part A1 of the liner are presented under a compressive deformation of 1 mm. These graphs compare the mechanical responses of the same geometric Area simulated with different liner materials, including Silicone, EL50, and TPU with auxetic architecture.

The force–displacement behavior of the silicone and EL50 materials exhibits a linear trend. Among these, silicone demonstrates the lowest reaction force, registering approximately 0.07 kN at 1 mm displacement, indicative of its low stiffness and limited energy absorption capacity. In contrast, the EL50 liner presents a steeper slope, reaching approximately 0.9 kN under the same displacement, reflecting its relatively higher resistance to compressive deformation.

In the case of the TPU-based auxetic structure, the force–displacement curve displays a distinct non-linear and asymmetric pattern, characteristic of hyperelastic materials. Notably, the loading and unloading paths differ due to the Mullins effect, which is incorporated into the finite element model. This results in a visible hysteresis loop, indicative of both energy absorption and dissipation capabilities of the auxetic TPU design.

In the evaluation of liner materials for lower limb prosthetic applications for part A1, as demonstrated in Table 3, the silicone liner exhibited the lowest absorbed energy (0.044 J) with a specific energy absorption (SEA) of 0.009 J/g. This suggests minimal deformation-induced energy dissipation and reflects the material's linear elastic and low-stiffness behavior. The EL50-based liner demonstrated a significantly improved performance, absorbing 0.74 J of energy and achieving a SEA of 0.15 J/g. This can be attributed to EL50's higher modulus and enhanced strain-hardening properties, enabling more efficient energy accommodation during loading. In contrast, the auxetic TPU structure, specifically engineered with negative Poisson's ratio behavior, absorbed 0.43 J of energy with a SEA of 0.24 J/g. Although its absolute energy absorption is lower than EL50, the structure achieved a remarkably better SEA, indicating efficient performance in terms of energy absorption relative to mass. Furthermore, this sample dissipated 0.11 J of energy, corresponding to a specific dissipated energy (SDE) of 0.07 J/g, highlighting its capability for cyclic energy dissipation, a critical factor for comfort and protection during dynamic gait cycles.

As illustrated in Fig. 7b, the von Mises stress distribution within the liner–socket assembly for the designed part A1 is analyzed under a

compressive load of 850 N, representing the maximum anticipated force applied by the user's body weight. Three different liner materials, Silicone, EL50, and TPU with an auxetic structure, are investigated, while the socket is uniformly simulated using PA12 across all cases.

The simulation results clearly reveal that the auxetic TPU liner exhibits a more uniform and lower stress distribution compared to conventional materials. Specifically, the stress magnitude in the TPU auxetic liner ranged from 0.02 MPa to 0.06 MPa, with the peak stress observed at approximately 0.09 MPa. In contrast, EL50 and Silicone liners exhibited significantly higher maximum localized stresses, reaching 0.12 MPa and ranging between 0.11 and 0.12 MPa, respectively.

Crucially, these results emphasize that liner design and material properties not only influence the stress levels within the liner itself but also directly impact stress transmission to the socket. The PA12 socket paired with the TPU auxetic liner experienced the lowest peak stress of 1.27 MPa, whereas the sockets combined with EL50 and Silicone liners showed peak stresses of 1.76 MPa and 1.59 MPa, respectively. This stress reduction in the socket when using an auxetic liner suggests that the energy-absorbing and stress-distributing capabilities of the auxetic structure effectively mitigate load transfer to the rigid socket component.

5.2. Liner, Area A2 and A3

As depicted in Fig. 8a, the force–displacement curves for the specifically designed part corresponding to areas A2 and A3, representing the anterior distal tibial end and distal fibular end, respectively, are illustrated under compressive cyclic loading. Due to the identical geometric dimensions considered in the design of parts A2 and A3, the simulation results for both parts are nearly indistinguishable, and thus are collectively represented by a single curve.

The results clearly demonstrate that the auxetic liner simulated with EL50 exhibits the highest reaction force, exceeding 0.6 kN at 1 mm displacement. In comparison, liners simulated with Silicone, and TPU with auxetic behavior reach reaction forces of approximately 0.05 kN and 0.3 kN, respectively, at the same displacement level.

In case of energy absorption and dissipation, as shown in Table 3.

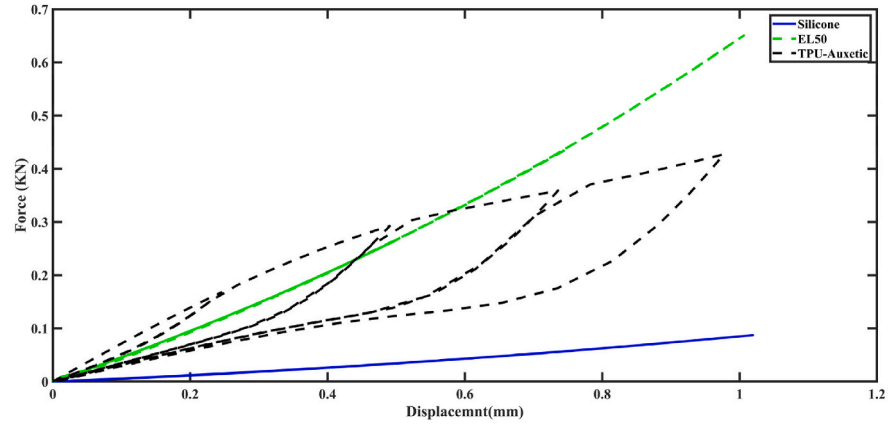

a)

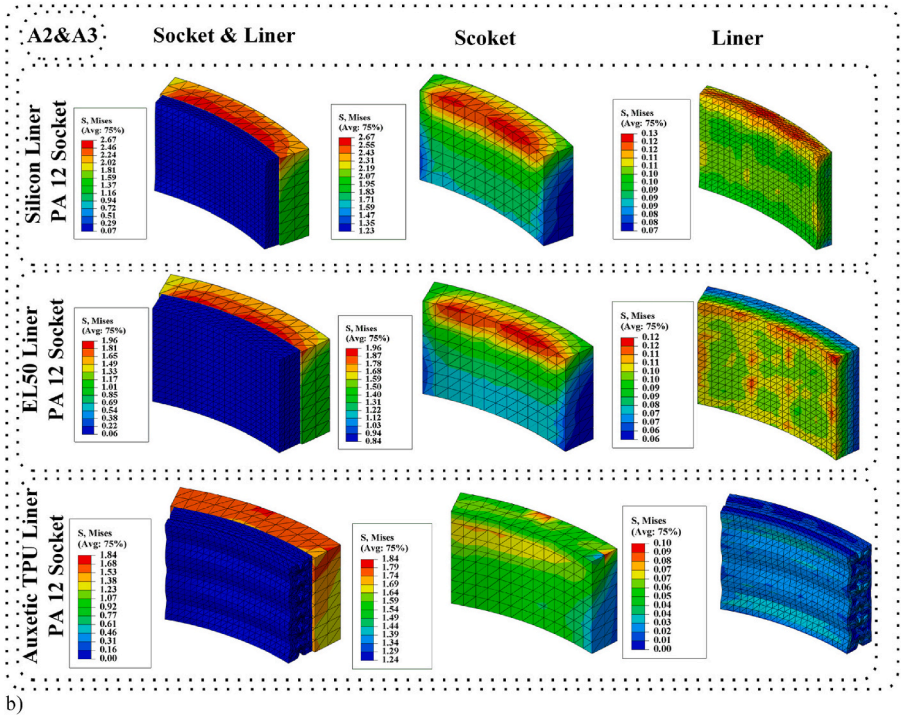

b)

Fig. 8. Simulation results for Part A2 and A3, a) Force-Displacement under 20 % strain, b) Von Mises stress distribution for the sample liner with Silicone and EL50 material, and auxetic liner with TPU material and socket with PA12 material.

The silicone liner, as expected, showed limited mechanical energy absorption, with an absorbed energy of only 0.039 J and a SEA of 0.023 J/g. This relatively low value is consistent with the inherently soft and highly elastic nature of silicone, which, while offering compliance, lacks capacity for significant energy accommodation or dissipation. The EL50 liner, with the same geometry and mass (1.7 g), absorbed 0.29 J of energy, yielding a SEA of 0.17 J/g. This represents a substantial improvement over silicone and is reflective of EL50's higher modulus and capacity to resist deformation while still providing resilience during load cycles. The auxetic TPU liner, designed with a geometry capable of re-entrant deformation mechanisms, showed both absorbed energy of 0.41 J and dissipated energy of 0.12 J. The corresponding SEA is 0.69 J/g and SDE is 0.20 J/g, outperforming both silicone and EL50 in terms of both total absorbed and dissipated energy per unit mass.

As illustrated in Fig. 8b, the von Mises stress distributions for the designed liner part corresponding to areas A2 and A3, which represent the anterior distal tibial end and distal fibular end, are presented under identical boundary conditions. The figure includes comparative stress maps for three different liner materials: Silicone, EL50, and TPU with auxetic architecture, all embedded within a socket simulated with PA-12.

The results indicate that the highest localized stress within the liner occurs in the Silicone configuration, with a peak von Mises stress reaching approximately 0.13 MPa. The EL50 liner follows with a peak stress of 0.12 MPa, while the TPU-based auxetic liner demonstrates the lowest peak stress, approximately 0.10 MPa. This reduction in stress in the TPU liner confirms its superior ability to redistribute mechanical loads, thereby alleviating pressure concentration on the sensitive distal tibial and fibular ends.

In addition to reducing internal stress within the liner, the auxetic TPU structure also contributes to decreased stress levels in the surrounding socket. Specifically, the maximum von Mises stress observed in the PA-12 socket paired with the TPU liner is 1.84 MPa, which is substantially lower than the stress levels in sockets paired with other liner materials. For instance, the socket coupled with the Silicone liner experiences a maximum stress of 2.67 MPa, while that of the EL50 configuration reaches 1.96 MPa.

5.3. Liner Area A4

As depicted in Fig. 9a, the mechanical response of part A4, corresponding to the patellar Area of the residual limb, is analyzed through force-displacement behavior under cyclic compression. This part is critical due to its direct alignment with the patella bone, an Area highly sensitive to localized pressure during ambulation and weight-bearing. The graph illustrates the force-displacement curves for three different liner materials, Silicone, EL50, and TPU with an auxetic architecture, each subjected to four loading-unloading cycles, simulating realistic prosthetic gait dynamics. The displacement is plotted up to 1 mm, which corresponds to the maximum applied strain considered in this study.

As illustrated in Fig. 9a, the force–displacement curves for Part A4, designed for the patellar area, are compared for three liner materials: Silicone, EL50, and auxetic-structured TPU. Among these, the EL50 material demonstrated the highest reaction force, reaching approximately 7 kN at 1 mm displacement. In contrast, the silicone liner exhibited the softest mechanical response, with a nearly linear profile and a maximum force of less than 0.6 kN for the same displacement. The TPU liner with an auxetic structure displayed a non-linear and cyclic response, indicative of both energy absorption and dissipation. Its maximum force at 1 mm displacement reached around 0.9 kN, with visible variations in force across different loading cycles. This cyclic behavior suggests enhanced mechanical adaptability, making it a suitable candidate for applications in highly mobile areas like the anterior patella.

It is noteworthy that, unlike the other parts (A1–A3), the simulation of Part A4 is conducted in the absence of the socket. This is due to its anatomical location on the anterior side of the residual limb, which interfaces directly with the liner and does not require additional socket

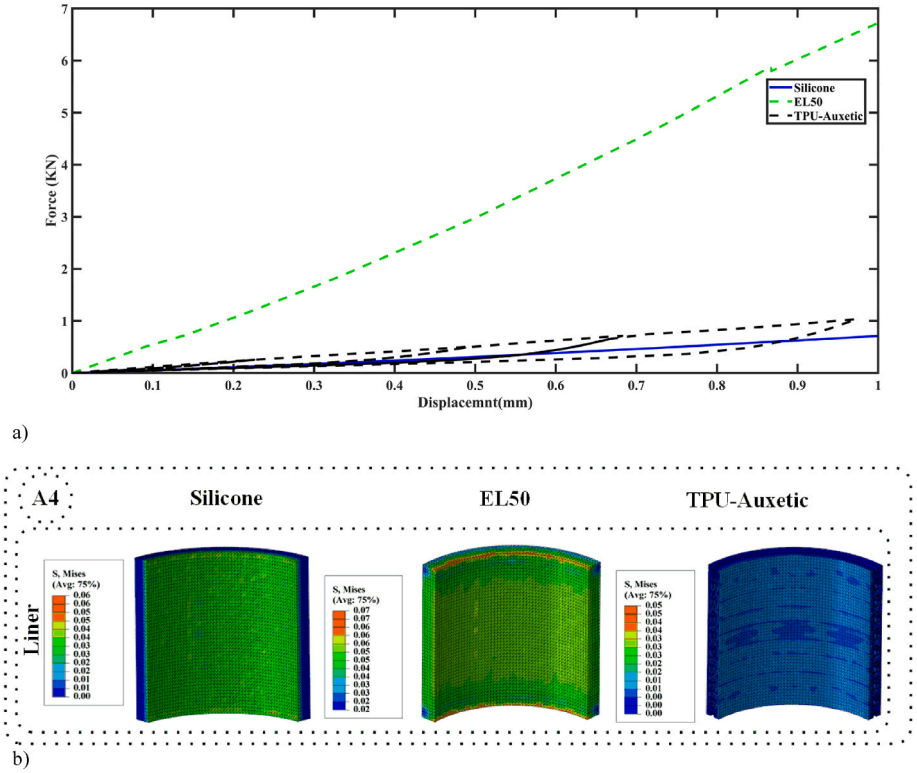

Fig. 9. Simulation results for Part A4, a) Force-Displacement under 20 % strain, b) Von Mises stress distribution for the sample liner with Silicone and material, and EL50 auxetic liner with TPU material.

coverage. As such, the observed differences in mechanical behavior highlight the independent performance of the liner material in the absence of structural reinforcement from the socket.

In terms of energy metrics regarding part A4, the Silicone liner absorbed 0.326 J of energy, resulting in a SEA of 0.022 J/g. Although the absolute energy absorbed is higher than in smaller samples (due to increased mass), the SEA remained low, consistent with silicone's elastic but non-dissipative nature. This reinforces its limited ability to buffer impact energy effectively, even when scaled up. The EL50 liner absorbed 3.13 J, producing a SEA of 0.21 J/g. This marked improvement reflects both the material's inherent toughness and its better resistance to deformation under stress.

The designed Auxetic Structure with TPU, despite a lower mass (5.29 g), achieved a comparable absorbed energy of 0.75 J and dissipated energy of 0.24 J. This resulted in a SEA of 0.14 J/g and SDE of 0.04 J/g. Although slightly lower in SEA than EL50 in this case, the presence of both absorption and dissipation mechanisms indicates a more balanced and advanced mechanical response. This analysis shows that while EL50 achieves the highest SEA in this sample, the auxetic TPU liner offers a superior combination of energy absorption and dissipation per unit mass, providing enhanced dynamic comfort and resilience under cyclic loading. Moreover, the TPU-based auxetic structure achieves high performance at a lower weight, which is crucial for reducing the mechanical burden on amputees during extended use.

As shown in Fig. 9b, the von Mises stress distribution for part A4, corresponding to the patellar Area, is evaluated across three liner configurations: Silicone, EL50, and auxetic TPU. This part is particularly important due to its close contact with the residual patella, a site prone to discomfort or pressure-induced injuries if not properly supported.

The stress contours reveal that the auxetic TPU liner exhibits superior stress management capabilities, especially in areas directly interfacing with the residual limb. Despite internal stresses reaching up to 0.05 MPa in some confined areas of the structure, particularly away from skin contact areas, the actual contact area experiences significantly lower stress, typically around 20 kPa. This behavior highlights the efficiency of the auxetic lattice geometry in redistributing internal stress away from sensitive contact surfaces. In contrast, both EL50 and Silicone liners show their peak stress values directly at the interface with the residual limb. The maximum stress at the contact surface for the EL50 liner reaches approximately 70 kPa, while the Silicone liner records around 60 kPa, indicating a relatively poor distribution of mechanical loads. This concentration of stress at the skin interface may lead to discomfort, irritation, or long-term soft tissue damage during extended prosthetic use.

The comparative assessment of four liner samples, ranging in mass, material composition, and structural design, revealed distinct mechanical behaviors with direct implications for prosthetic comfort, pressure distribution, and user safety.

Across all samples, traditional silicone liners consistently exhibited the lowest values, ranging from 0.009 to 0.023 J/g, with negligible energy dissipation. This linear elastic behavior, while offering softness and conformity, suggests limited impact mitigation potential. The material's low resilience under dynamic loading highlights its vulnerability to stress concentration at the skin-liner interface, potentially compromising long-term comfort in high-activity or cyclic load scenarios.

Most notably, the TPU-based liners with auxetic lattice structures demonstrated a superior multifunctional performance. While absolute SEA values ranged from 0.14 to 0.69 J/g, these designs uniquely offered both energy absorption and energy dissipation, as evidenced by their SDE values. These behaviors are a direct consequence of the negative Poisson's ratio and mechanical adaptability of the auxetic metamaterial geometry, which enables efficient energy redistribution, reduces peak stress at contact areas, and enhances comfort through uniform load transmission.

Furthermore, stress analysis clearly revealed that auxetic TPU liners exhibited significantly lower localized stress concentrations at the limb-liner interface, especially compared to traditional silicone and EL50-based liners. This stress-relieving capability not only contributes to increased biomechanical comfort for the amputee but also minimizes the risk of skin breakdown, pressure sores, and discomfort during long-term use.

Additionally, the auxetic liners demonstrated lower internal stress levels within their structural body, indicating improved mechanical integrity and resistance to failure during cyclic or repeated loading. This advantage not only enhances user comfort but also contributes to greater durability and structural reliability in real-life prosthetic applications.

In summary, the results clearly support the hypothesis that auxetic metamaterial-based liners, particularly those manufactured from hyperelastic TPU, offer a marked biomechanical and structural advantage over conventional materials, not only by reducing contact stress but also by enhancing energy dissipation, structural integrity, and adaptive load response. These findings position structured auxetic materials as a promising foundation for the next generation of user-centric, high-performance prosthetic interface systems.

5.4. Parts 5 and 6 of the socket

Building upon previous investigations and considering the mechanical function of prosthetic sockets, which must structurally interface with the external environment, higher stiffness materials are typically preferred. For this purpose, PA-12 and ABS are selected to simulate parts 5 and 6, representing rigid socket prototypes with and without auxetic design features, respectively.

As shown in Fig. 10a, the force-displacement behavior of these two samples is compared. The blue curve, corresponding to the auxetic design made of PA-12, shows an under 10 peak force response under 1 mm displacement, indicating more compliant energy behavior under compressive loads. In contrast, the conventional socket simulated with ABS (green curve) demonstrated a significantly higher force of approximately 10 KN, indicating a stiffer but more brittle mechanical response.

In terms of stress analysis (Fig. 10b), the auxetic PA-12 socket, which features an embedded auxetic lattice within a hemispherical shell, exhibited significantly lower stress concentrations. The maximum von Mises stress in the auxetic design is limited to 5.6 MPa, with surface stress values near the liner-socket interface ranging from 0.5 to 0.9 MPa. In comparison, the conventional ABS socket experienced a peak von Mises stress of 11.7 MPa, with surface contact stress values between 5.5 and 11.7 MPa, nearly double those of the auxetic design.

These stress differentials clearly demonstrate the mechanical advantage of incorporating auxetic geometry into socket structures, particularly in terms of stress distribution, energy redirection, and reduction of stress risers at the prosthetic interface.

Furthermore, a comparison of energy absorption, energy dissipation, and mass for both samples are presented in Table 3. The total absorbed energy of the ABS socket (9.469 J) is slightly higher than that of the PA-12 auxetic socket (7.22 J), which may initially suggest higher stiffness or resistance to deformation in the ABS model. However, this difference must be interpreted in the context of mass. When normalized by mass, the SEA of the auxetic PA-12 socket is 0.14 J/g, which is approximately 38 % higher than that of the ABS socket (0.101 J/g). This indicates that the auxetic design is more efficient in absorbing energy relative to its weight, a critical factor in prosthetic design where weight minimization is key to user comfort. The auxetic socket is deliberately engineered using a PA-12 polymer matrix with an internal auxetic metamaterial geometry to reduce stress concentrations and improve energy distribution. The intention is to develop a socket that performs better, providing a softer, more conformal fit while still maintaining adequate rigidity to resist environmental impact forces. Although the total absorbed energy in the conventional ABS socket is slightly higher, the auxetic PA-12 socket clearly outperforms in SEA, confirming its superior energy efficiency per unit weight. This is crucial in socket design, where weight reduction directly contributes to patient comfort, making it ideal for

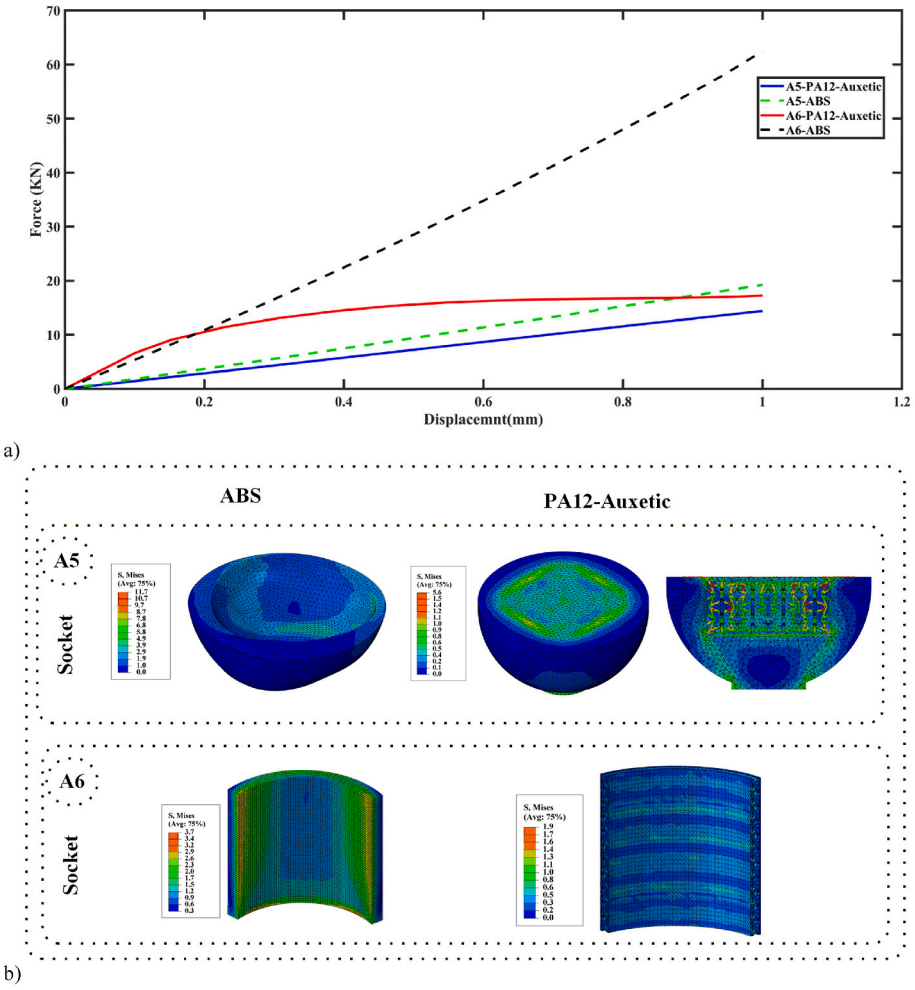

Fig. 10. Simulation results for Part A5 and A6, a) Force-Displacement under 20 % strain, b) Von Mises stress distribution for the sample socket with ABS material, and auxetic socket with PA12 material.

structural integrity while still promoting stress delocalization a trait previously confirmed by stress contour plots. These findings reinforce the value of combining auxetic architectures with PA-12 for advanced prosthetic socket design.

The mechanical performance of Part A6, designed with an auxetic structure using PA-12 material, is comprehensively evaluated against a conventional ABS socket to assess the implications of auxetic geometry and material flexibility on stress mitigation and load response in lower limb prosthetic applications which overlays the tibial crest and is often subjected to compressive forces in rigid socket designs.

As illustrated in Fig. 10a, the force–displacement behavior of both sockets under 20 % compressive strain is distinctly different. The red curve, corresponding to the auxetic PA-12 socket, exhibits a nonlinear profile that reflects the plastic deformation behavior of PA-12. Notably, the maximum reaction force reached approximately 10 kN, demonstrating a more compliant load response. In contrast, the black curve, associated with the conventional ABS socket, shows a significantly stiffer profile, with a peak force of nearly 60 kN under the same strain.

As shown in Fig. 10b, the maximum von Mises stress under 850 N force in the auxetic PA-12 socket Part A5 is observed to be approximately 5.6 MPa, which is significantly lower than the 11.7 MPa recorded in the ABS socket. Furthermore, the stress distribution across the contact interface between the socket and liner in the auxetic design Part A6 is more uniform, ranging from 0.2 MPa to 0.9 MPa, compared to the ABS socket, where localized stress concentrations reached the upper bound of 3.7 MPa. This more homogeneous stress distribution is likely to enhance comfort and reduce pressure-related complications for amputees.

According to Table 3, SEA for the auxetic PA-12 socket Part A5 is 0.14 J/g, while the conventional ABS socket showed an SEA of only 0.101 J/g. The total absorbed energy of Part A6 with PA-12 design is 13.23 J for a mass of 1.85 g, compared to 29.103 J absorbed by the ABS structure with a mass of 18 g, further emphasizing the lightweight efficiency and mechanical advantage of the auxetic socket.

This analysis demonstrates the remarkable potential of auxetic architectures in socket design for prosthetic limbs. The auxetic socket simulated of PA-12 not only shows superior energy absorption and mass efficiency but also achieves a dramatic reduction in both stress intensity and concentration at critical contact areas. These findings validate the auxetic–PA-12 combination as a highly promising candidate for improving mechanical comfort and performance in next-generation prosthetic interfaces.

5.5. Stress distribution evaluation of liner designs incorporating auxetic structures

Following the design and analysis of parts A1 to A4, these components are integrated into a complete 3D liner model for comprehensive evaluation. For comparison purposes, a basic silicone liner (conventional structure) is also simulated under identical boundary and loading conditions in ABAQUS. In addition, a fully auxetic liner constructed entirely from TPU is modeled and analyzed to investigate the effects of

uniform auxetic geometry throughout the liner structure.

All TPU-based liners, including both the four-Area auxetic liner and the fully auxetic liner, are constructed from auxetic lattice units specifically designed for the pressure-sensitive Areas of the residual limb. As illustrated in Fig. 11, the stress response is assessed across four clinically significant areas. To facilitate a localized performance assessment, 80 % of the total applied load is distributed among these four key areas, simulating realistic pressure concentration patterns during gait, while the remaining 20 % of the total load is applied to other areas of the liners. The total force applied amounts to 850 N.

The results highlight the superior stress-mitigating potential of the auxetic designs:

In the conventional silicone liner, maximum stresses in the critical Areas reached 50 kPa, with pronounced stress concentration particularly near the distal tibial and fibular areas. In the four-area auxetic TPU liner, maximum stress in the contact interfaces dropped significantly to approximately 24 kPa, particularly at the junctions between auxetic and non-auxetic Areas. For the fully auxetic TPU liner, peak stress is further reduced to 18 kPa, representing the lowest stress magnitude among all three designs. These results validate the design rationale and biomechanical efficacy of auxetic liners, especially the fully auxetic variant, which exhibited the most uniform and minimized stress distribution. Furthermore, the four-area TPU auxetic liner also demonstrated substantial improvements compared to the conventional silicone liner, particularly in high-pressure anatomical Areas, confirming its clinical potential for enhanced user comfort and skin protection.

5.6. Stress analysis and biomechanical implications of three socket designs

To investigate the biomechanical performance of prosthetic sockets, three distinct designs are analyzed as shown in Fig. 12: (1) a conventional socket simulated with ABS, (2) a PA12 socket incorporating two auxetic areas at anatomically sensitive Areas A5 and A6, and (3) a fully auxetic PA12 socket. All designs are subjected to finite element analysis under standardized loading conditions to assess von Mises stress distribution and structural performance.

The baseline socket design, simulated with ABS without any auxetic modifications, exhibited a peak von Mises stress of 6.45 MPa and 7.5 MPa in areas A5 and A6, respectively. Stress concentration is notably high in areas A5 and A6, locations commonly associated with discomfort and mechanical mismatch in amputees due to bony protrusions or irregular soft-tissue profiles. These values align with previous studies on conventional socket stress profiles, confirming the mechanical limitations of homogeneous socket structures(Barreto et al., 2022).

In the second configuration, targeted auxetic patterns are integrated into two critical anatomical areas (A5 and A6), utilizing PA12 material. This design resulted in a significant reduction of peak stress values, down to 3.6 MPa and 4.1 MPa in areas A5 and A6. Importantly, stress maps demonstrated a clear redistribution of load within the auxetic areas, indicating their effectiveness in minimizing localized pressure. These areas functioned as compliant buffers, enhancing mechanical compatibility between the rigid socket wall and the underlying residual limb anatomy.

The fully auxetic socket simulated with PA12 auxetic lattice showed the most impressive biomechanical performance. Peak von Mises stress

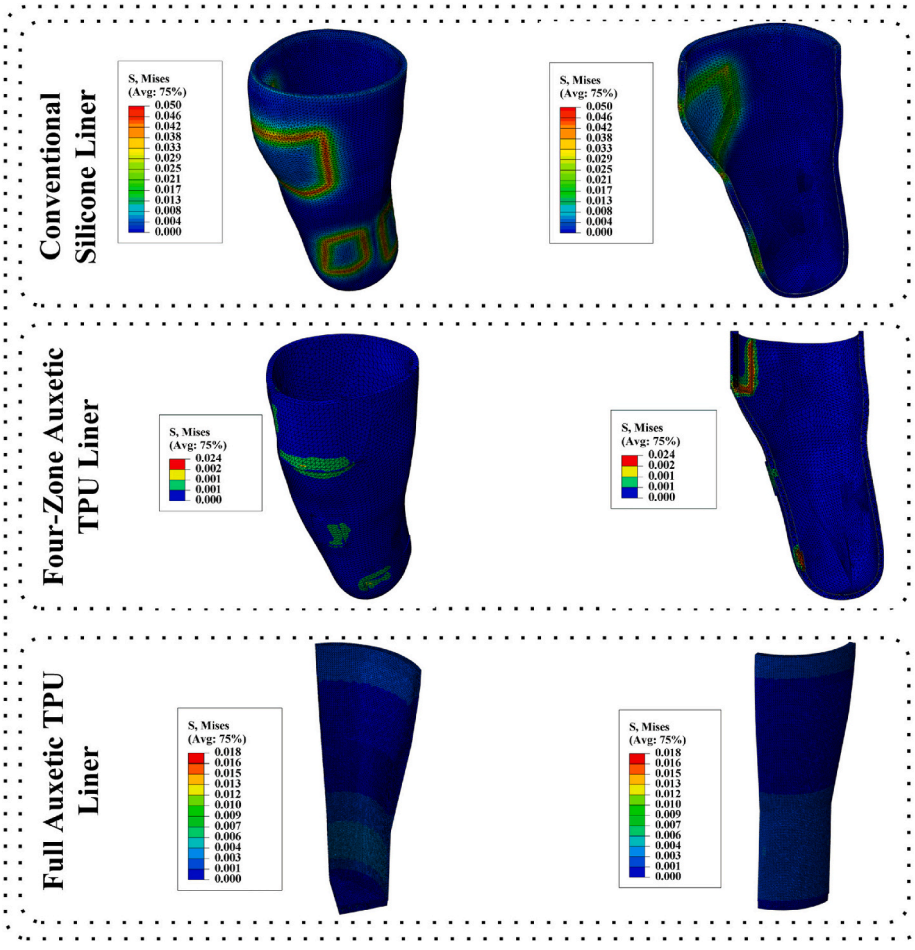

Fig. 11. Simulation results, Von Mises stress distribution for the sample liner with silicone material, and four-zone auxetic and full auxetic liner with TPU material.

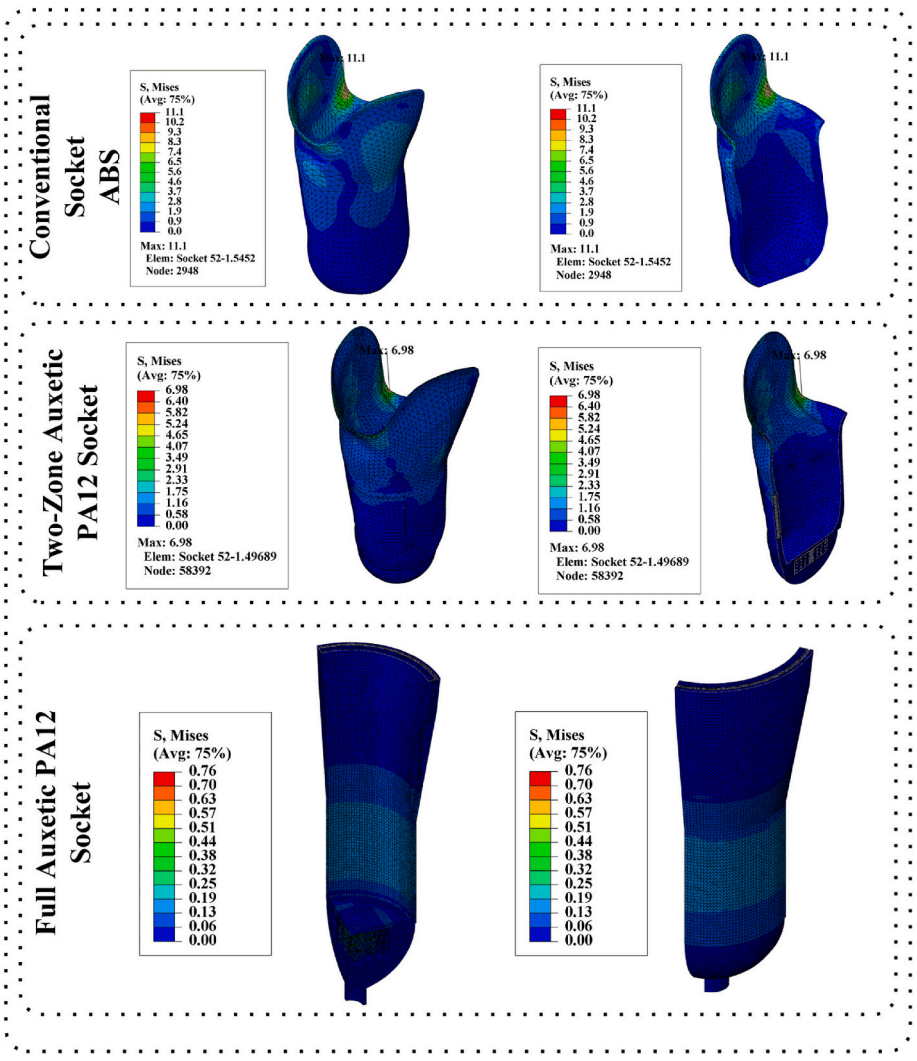

Fig. 12. Simulation results, Von Mises stress distribution for the conventional socket with ABS material, and two-zone auxetic and full auxetic socket with PA12 material.

is reduced to 0.76 MPa, highlighting a drastic improvement in stress attenuation compared to both previous models. The full-auxetic PA-12 socket supplementary reduced these peaks to just 0.44 MPa and 0.76 MPa in area A5 and A6. Additionally, the stress distribution is markedly uniform, with no discernible hot spots or sharp gradients, factors that contribute to improved comfort, reduced risk of soft tissue injury, and better limb-socket interaction.

Furthermore, the fully auxetic socket benefits from substantially lower mass compared to the conventional ABS model, due to the inherent lattice structure and material properties of PA12. This weight reduction enhances balance, stability, and long-term wearability. From a manufacturing perspective, the auxetic design is well-suited for AM, potentially reducing production costs and material. The progressive integration of auxetic architectures, either locally or fully, into prosthetic socket designs has demonstrated a significant biomechanical advantage. The fully auxetic PA12 socket, in particular, offers the optimal combination of stress reduction, comfort, and structural efficiency, making it a promising candidate for next-generation lower-limb prosthetic interfaces.

6. Conclusion

Substantial biomechanical and structural benefits of integrating auxetic metamaterial geometries into prosthetic liners and sockets were demonstrated. Comparative finite-element analyses across configurations A1-A6 showed consistent reductions in peak von Mises stresses within load-bearing and pressure-sensitive regions when auxetic structures were employed.

For the liner, transitioning from a conventional design to a TPU-based four-region auxetic configuration lowered maximum stresses in A1-A4 from 50, 46, 46, and 42 kPa to 24, 24, 20, and 18 kPa, respectively, reductions of up to ~57 %. The fully auxetic TPU liner achieved peaks of 18, 16, 18, and 13 kPa in the same regions, corresponding to reductions of ~64 %, ~65 %, ~61 %, and ~69 % relative to baseline. These decreases directly address comfort and tissue health by mitigating pressure concentrations on anatomical landmarks such as the tibial crest and fibular head. For sockets, the incorporation of auxetic regions in PA-12 designs significantly lowered stresses compared with ABS conventional sockets. In regions A5 and A6, peak stresses dropped from 6.45 MPa to 7.50 MPa (ABS) to 3.60 MPa and 4.10 MPa for the two-region auxetic PA-12 socket (~44 % and ~45 % reductions). The fully auxetic PA-12 socket further reduced these peaks to 0.76 MPa and 0.44 MPa (~88 % and ~94 % reductions). These outcomes indicate strong potential to improve user comfort, reduce residual-limb tissue damage, and prolong prosthetic use without discomfort. Energy-absorption analyses reinforced these findings. Auxetic TPU liners exhibited higher SEA and SDE than their conventional counterparts, indicating enhanced shock mitigation and greater energy return during gait. Similarly, the

PA-12 auxetic socket showed an effective balance of stiffness and compliance, offering improved load distribution without sacrificing structural integrity.

A comparison of current results with previous studies on metamaterial-based prosthetic interfaces shows that the proposed auxetic designs achieve significantly lower stress levels. Barreto et al. (2022) reported peak pressures in transtibial sockets of 6.25–13.7 MPa with conformal lattice structures, while the fully auxetic PA12 socket in this study reduced peak von Mises stresses to 0.76 MPa and 0.44 MPa. Devin et al. (2024) found peak pressures of 50–90 kPa in metamaterial liners, and Brown et al. (Brown et al. (2021) reported pressures of 70–110 kPa with a single-layer metamaterial insert, while the auxetic TPU liner in this study yielded stresses of just 18–24 kPa.

Overall, the integration of auxetic geometries into liners and sockets presents a promising approach to prosthetic interface design, balancing biomechanical performance, user comfort, and structural durability. By targeting mechanical properties in anatomically critical zones, notable reductions in harmful peak stresses were achieved while maintaining or enhancing energy management. These results validate the efficacy of auxetic metamaterials in prosthetic applications and motivate future work on patient-specific optimization, scalable additive manufacturing, and long-term clinical evaluation.

CRediT authorship contribution statement

Mahdi Bodaghi: Writing – review & editing, Supervision, Resources, Project administration, Methodology, Investigation, Funding acquisition, Conceptualization, Data curation. **Saman Jolaiy:** Writing – review & editing, Writing – original draft, Visualization, Validation, Methodology, Investigation, Formal analysis, Data curation. **Kaveh Rahmani:** Writing – review & editing, Methodology, Investigation, Data curation. **Sheng Li:** Writing – review & editing, Methodology, Investigation, Data curation. **Fei Gao:** Writing – review & editing, Supervision, Resources, Methodology, Investigation, Funding acquisition. **Ali Zolfagharian:** Writing – review & editing, Supervision, Methodology, Investigation, Funding acquisition.

Compliance with ethics guidelines

This article does not contain any studies with human or animal subjects performed by any of the authors.

Declaration of competing interest

The authors declare that they have no known competing financial interests or personal relationships that could have appeared to influence the work reported in this paper.

Acknowledgments

The authors acknowledge the support by the UK Engineering and Physical Sciences Research Council (EPSRC) (award no.: EP/Y011457/1), the Shenzhen basic research key project (project no.: JCYJ20220818101407016), and the Australian Research Council under the Discovery Early Career Award [project no.: DE240100960].

Data availability

Data will be made available on request.

References

Alomarah, A., et al., 2020a. Dynamic performance of auxetic structures: experiments and simulation. Smart Mater. Struct. 29 (5), 055031.
Alomarah, A., et al., 2020b. Compressive properties of 3D printed auxetic structures: experimental and numerical studies. Virtual Phys. Prototyp. 15 (1), 1–21.
Arun, S., Kanagaraj, S., 2016. Performance enhancement of epoxy based sandwich composites using multiwalled carbon nanotubes for the application of sockets in trans-femoral amputees. J. Mech. Behav. Biomed. Mater. 59, 1–10.
Baldock, M., et al., 2023. Adjustable prosthetic sockets: a systematic review of industrial and research design characteristics and their justifications. J. NeuroEng. Rehabil. 20 (1), 147.
Barreto, M.A., et al., 2022. The use of conformal lattice metamaterials for relieving stress in lower limb sockets: a numerical and exploratory study. Proc. IME H J. Eng. Med. 236 (11), 1635–1645.
Basha, S.A., Agrawal, A.K., Sarkar, D., 2021. Tailor-made design, fabrication and validation of SrO doped nanostructured ZTA ceramic femoral head–acetabular socket liner assembly. J. Mech. Behav. Biomed. Mater. 114, 104178.
Bates, S.R., Farrow, I.R., Trask, R.S., 2019. Compressive behaviour of 3D printed thermoplastic polyurethane honeycombs with graded densities. Mater. Des. 162, 130–142.
Brown, N., et al., 2020. Metamaterial design for targeted limb-socket interface pressure offloading in transtibial amputees. In: International Design Engineering Technical Conferences and Computers and Information in Engineering Conference. American Society of Mechanical Engineers.
Brown, N., et al., 2021. Design of a single layer metamaterial for pressure offloading of transtibial amputees. J. Biomech. Eng. 143 (5), 051001.
Devin, K.M., et al., 2024. Assessment of 3D printed mechanical metamaterials for prosthetic liners. Proc. IME H J. Eng. Med. 238 (3), 348–357.
Eshraghi, A., et al., 2013. 100 top-cited scientific papers in limb prosthetics. Biomed. Eng. Online 12, 1–12.
Fardan, M.F., et al., 2023. Revolutionizing prosthetic design with auxetic metamaterials and structures: a review of mechanical properties and limitations. Micromachines 14 (6), 1165.
García-Ávila, J., et al., 2024. Dynamic topology optimization of 3D-Printed transtibial orthopedic implant using tunable isotropic porous metamaterials. J. Mech. Behav. Biomed. Mater. 153, 106479.
Ghavidelnia, N., Bodaghi, M., Hedayati, R., 2020. Femur auxetic meta-implants with tuned micromotion distribution. Materials 14 (1), 114.
Ghavidelnia, N., Bodaghi, M., Hedayati, R., 2021. Idealized 3D auxetic mechanical metamaterial: an analytical, numerical, and experimental study. Materials 14 (4), 993.
Han, D., et al., 2022a. Lightweight auxetic metamaterials: design and characteristic study. Compos. Struct. 293, 115706.
Han, D., et al., 2022b. Experimental and computational investigations of novel 3D printed square tubular lattice metamaterials with negative Poisson's ratio. Addit. Manuf. 55, 102789.
Han, D., et al., 2025a. Experimental and numerical investigations of bio-inspired hollow re-entrant auxetic metamaterials manufactured using laser powder bed fusion. J. Mater. Res. Technol. 39, 4898–4912.
Han, D., et al., 2025b. Utilizing partially-curved-beam to improve stress response and energy absorption performance of auxetic lattice metamaterials. Thin-Walled Struct. 217, 113896.
Hasanzadeh, R., et al., 2025. Auxetic 3D printed metastructure stents for enhanced mechanical and structural performance and biocompatibility in coronary artery treatments. Acta Biomater.
Hedayati, R., et al., 2023. Analytical relationships for 2D Re-entrant auxetic metamaterials: an application to 3D printing flexible implants. J. Mech. Behav. Biomed. Mater. 143, 105938.
Jiang, D., et al., 2024. Advances in additive manufacturing of auxetic structures for biomedical applications. Mater. Today Commun., 110045
Johnston, R., Kazancı, Z., 2021. Analysis of additively manufactured (3D printed) dual-material auxetic structures under compression. Addit. Manuf. 38, 101783.
Jolaiy, S., et al., 2024a. Stability analysis of multi-trigger nano tube sandwich structures considering thermal and magnetic effects. Waves Random Complex Media 1–24.
Jolaiy, S., et al., 2024b. Limpet-inspired design and 3D/4D printing of sustainable sandwich panels: pioneering supreme resiliency, recoverability and repairability. Appl. Mater. Today 38, 102243.
Jolaiy, S., et al., 2025. Structure-negative poisson's ratio analysis and optimization in a novel additively manufactured polymeric hybrid auxetic metastructure via 3D printing, finite element analysis, and machine learning. Smart Mater. Struct.
Joseph, A., Mahesh, V., Harursampath, D., 2021. On the application of additive manufacturing methods for auxetic structures: a review. Advances in Manufacturing 9 (3), 342–368.
Kelkar, P.U., et al., 2020. Cellular auxetic structures for mechanical metamaterials: a review. Sensors 20 (11), 3132.
Klute, G.K., Glaister, B.C., Berge, J.S., 2010. Prosthetic liners for lower limb amputees: a review of the literature. Prosthet. Orthot. Int. 34 (2), 146–153.
Li, X., et al., 2019. Novel auxetic structures with enhanced mechanical properties. Extreme Mechanics Letters 27, 59–65.
Lvov, V.A., et al., 2022. Auxetic metamaterials for biomedical devices: current situation, main challenges, and research trends. Materials 15 (4), 1439.
Manz, S., et al., 2022. A review of user needs to drive the development of lower limb prostheses. J. NeuroEng. Rehabil. 19 (1), 119.
Mao, C., et al., 2025. Advanced topology optimisation for porous hip Implants: bridging in silico models and in vitro tests. Journal of the mechanical behavior of biomedical materials 170, pp. 107031–107031.
Meena, K., Singamneni, S., 2019. A new auxetic structure with significantly reduced stress concentration effects. Mater. Des. 173, 107779.
Miyata, Y., et al., 2022. Sustainable, affordable and functional: reimagining prosthetic liners in resource limited environments. Disabil. Rehabil. 44 (12), 2941–2947.

Nagarajan, Y.R., et al., 2024. Single polymer composites: an innovative solution for lower limb prosthetic sockets. Prosthesis 6 (3), 457–477.
Namvar, N., et al., 2022. Reversible energy absorption of elasto-plastic auxetic, hexagonal, and AuxHex structures fabricated by FDM 4D printing. Smart Mater. Struct. 31 (5), 055021.
Paternò, L., et al., 2018. Sockets for limb prostheses: a review of existing technologies and open challenges. IEEE (Inst. Electr. Electron. Eng.) Trans. Biomed. Eng. 65 (9), 1996–2010.
Paternò, L., et al., 2020. A personalised prosthetic liner with embedded sensor technology: a case study. Biomed. Eng. Online 19, 1–20.
Pezzin, L.E., et al., 2004. Use and satisfaction with prosthetic limb devices and related services. Archives of physical medicine and rehabilitation 85 (5), 723–729.
Plesec, V., Harih, G., 2023. Development of a generic numerical transtibial model for limb–prosthesis system evaluation. Applied Sciences 13 (4), 2339.
Price, M.A., Beckerle, P., Sup, F.C., 2019. Design optimization in lower limb prostheses: a review. IEEE Trans. Neural Syst. Rehabil. Eng. 27 (8), 1574–1588.
Quan, C., et al., 2020. 3d printed continuous fiber reinforced composite auxetic honeycomb structures. Compos. B Eng. 187, 107858.
Ren, X., et al., 2018. Auxetic metamaterials and structures: a review. Smart Mater. Struct. 27 (2), 023001.
Safari, R., Meier, M.R., 2015a. Systematic review of effects of current transtibial prosthetic socket designs—Part 1: qualitative outcomes. J. Rehabil. Res. Dev.
Safari, R., Meier, M.R., 2015b. Systematic review of effects of current transtibial prosthetic socket designs—Part 2: quantitative outcomes. J. Rehabil. Res. Dev.
Shirzad, M., et al., 2024. Design and optimization of bioinspired auxetic structure for biomedical applications. Eur. J. Mech. Solid. 103, 105139.
Veerabagu, U., Palza, H., Quero, F., 2022. Auxetic polymer-based mechanical metamaterials for biomedical applications. ACS Biomater. Sci. Eng. 8 (7), 2798–2824.
Wang, M., et al., 2022. Design of lower limb prosthetic sockets: a review. Expet Rev. Med. Dev. 19 (1), 63–73.
Yang, C., Vora, H.D., Chang, Y., 2018. Behavior of auxetic structures under compression and impact forces. Smart Mater. Struct. 27 (2), 025012.
Young, P.R., et al., 2023. Advances in the measurement of prosthetic socket interface mechanics: a review of technology, techniques, and a 20-year update. Expet Rev. Med. Dev. 20 (9), 729–739.
Yousefi, A., et al., 2023. 3D-Printed soft and hard meta-structures with supreme energy absorption and dissipation capacities in cyclic loading conditions. Adv. Eng. Mater. 25 (4), 2201189.